Semi-Analytic Modeling of Galaxy Formation

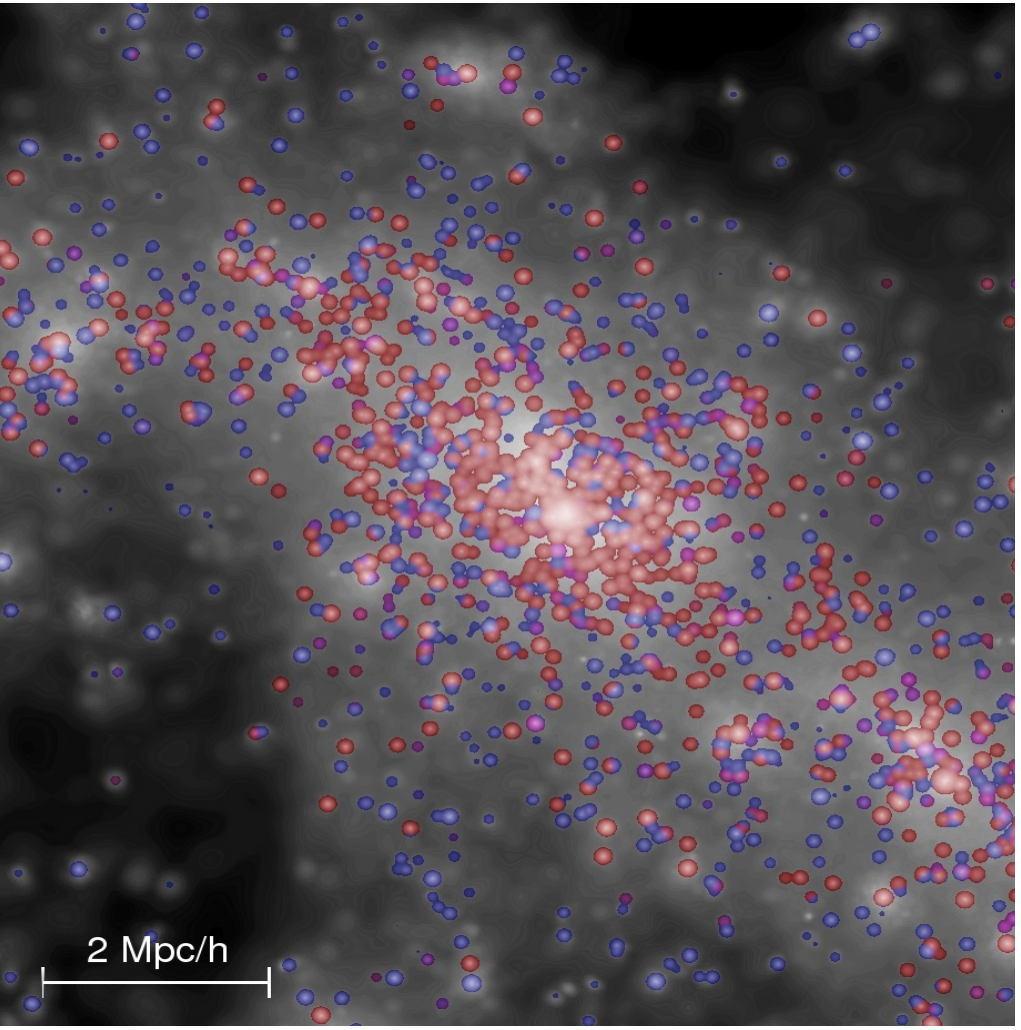

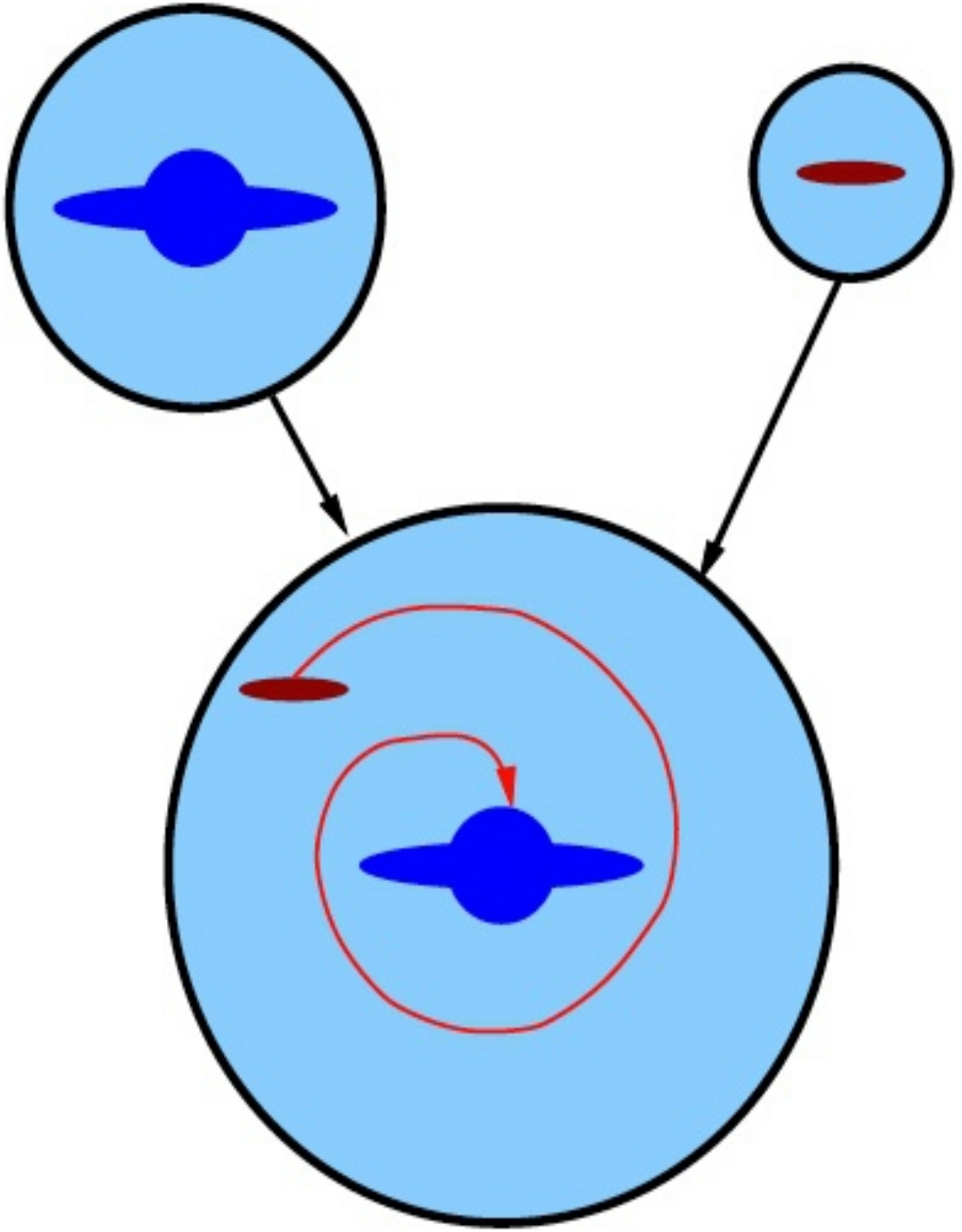

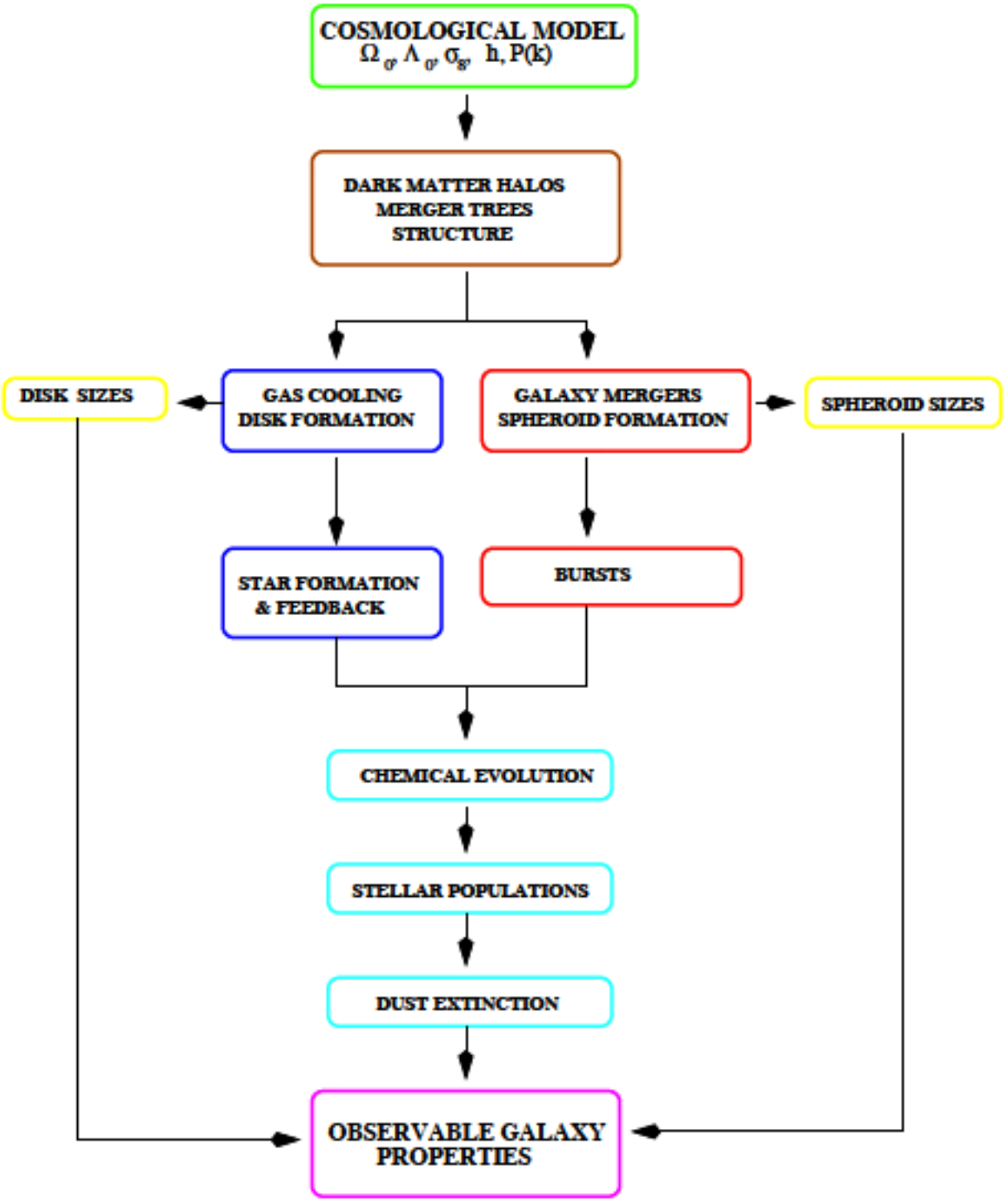
COSMOLOGICAL MODEL
$\Omega_0, \Lambda_0, \sigma_8$, h, P(k)
DARK MATTER HALOS
MERGER TREES
STRUCTURE
DISK SIZES
GAS COOLING
DISK FORMATION
GALAXY MERGERS
SPHEROID FORMATION
SPHEROID SIZES
STAR FORMATION
& FEEDBACK
BURSTS
CHEMICAL EVOLUTION
STELLAR POPULATIONS
DUST EXTINCTION
OBSERVABLE GALAXY
PROPERTIES

We build virtual catalogues of the galaxy population by implementing galaxy formation models on the stored output of two very large cosmological N-body simulations, the MS (Springel et al. 2005) and the MS-II (Boylan-Kolchin et al. 2009). Both simulations assume a ΛCDM cosmology with parameters based on a combined analysis of the 2dFGRS (Colless et al. 2001) and the first-year *WMAP* data (Spergel et al. 2003). The parameters are $\Omega_{\rm m} = 0.25$, $\Omega_{\rm b} = 0.045$, $\Omega_\Lambda = 0.75$, $n = 1$, $\sigma_8 = 0.9$ and $H_0 = 73\,{\rm km\,s^{-1}\,Mpc^{-1}}$. These cosmological parameters are not consistent with more recent analyses of the CMB data (e.g. Komatsu et al. 2010)

Both the MS and the MS-II trace 2160^3 particles from redshift 127 to the present day. The MS was carried out in a periodic box of side 685 Mpc and the MS-II in a box of side 137 Mpc. The corresponding particle masses are 1.18×10^9 and 9.45×10^6 $M_\odot$, respectively. The smallest haloes/subhaloes we consider contain 20 bound particles and it will turn out that the MS-II has just sufficient resolution to study dwarf galaxies as faint as those seen around the Milky Way. Conversely, the large volume of the MS makes it possible to study rare objects like rich clusters and bright quasar hosts. In addition, a comparison of the two simulations where both have good statistics allows us to study how the limited resolution of the MS affects its model galaxy populations.

Millennium Simulation I

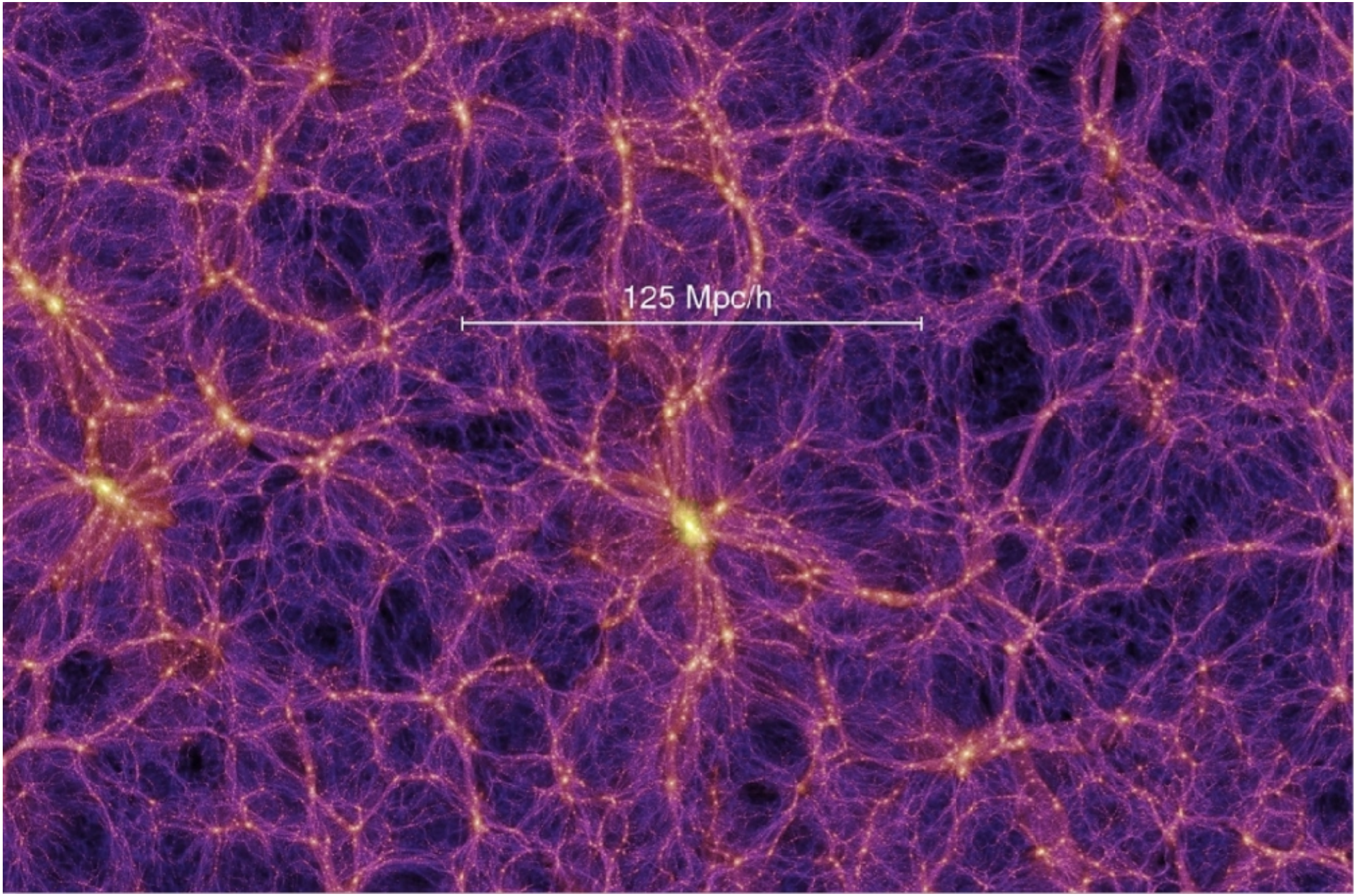

Millennium Simulation II

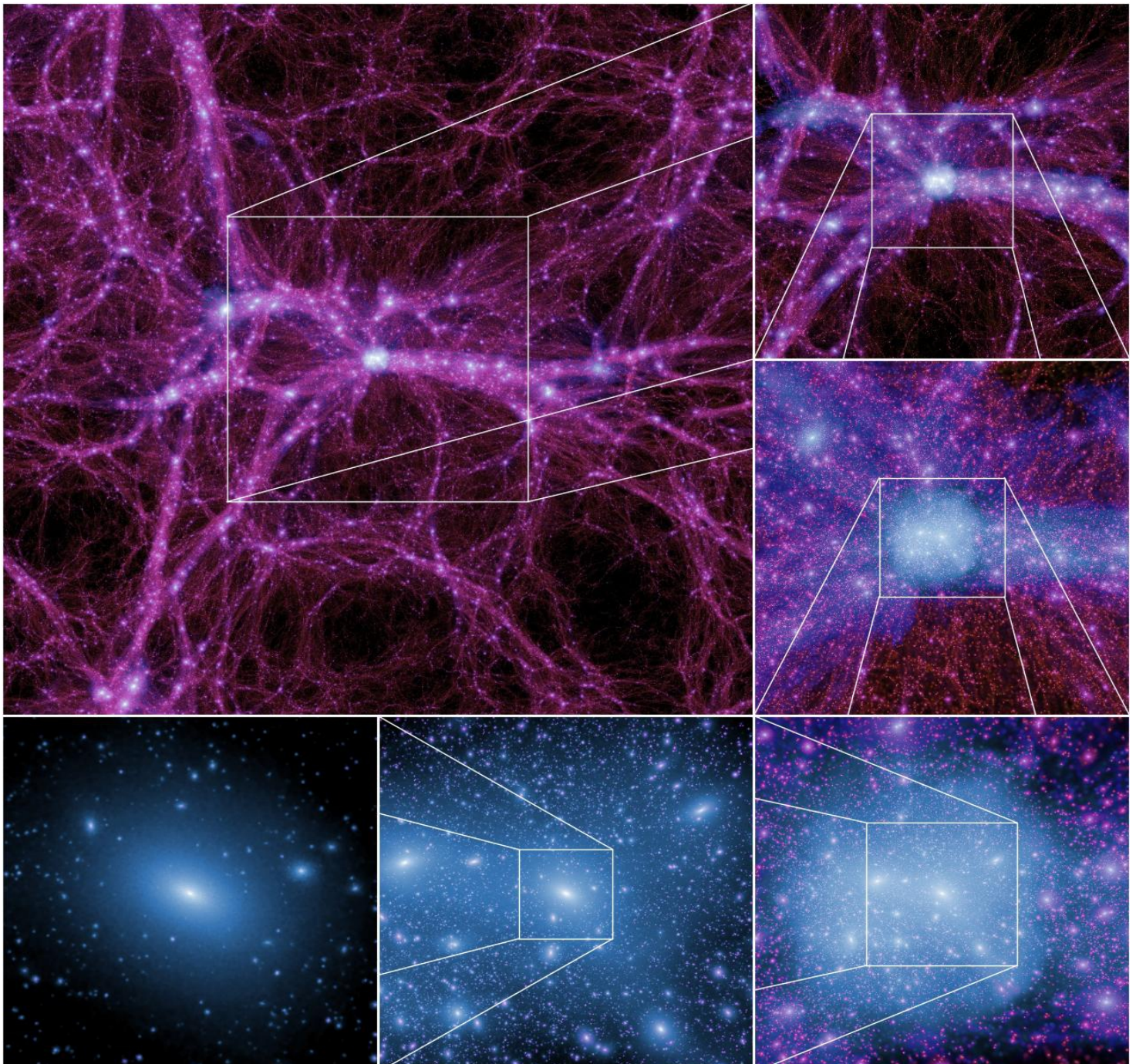

The particle data were stored at 64 and 68 times for the MS and the MS-II, respectively, with the last 60 being identical in the two simulations. At each output time, the post-processing pipeline produced a friends-of-friends (FOF) catalogue by linking particles with separation less than 0.2 of the mean value (Davis et al. 1985). The SUBFIND algorithm (Springel et al. 2001) was then applied to each FOF group to identify all its bound substructures (subhaloes).

our galaxy formation models are thus based on the growth and merging of the population of *subhaloes*, not on the growth and merging of the population of *haloes*. This is an important distinction which allows us to build much more realistic models for the galaxy population, in particular for its merging rates and its clustering, than would otherwise be the case.

“Traditional” Merger Tree

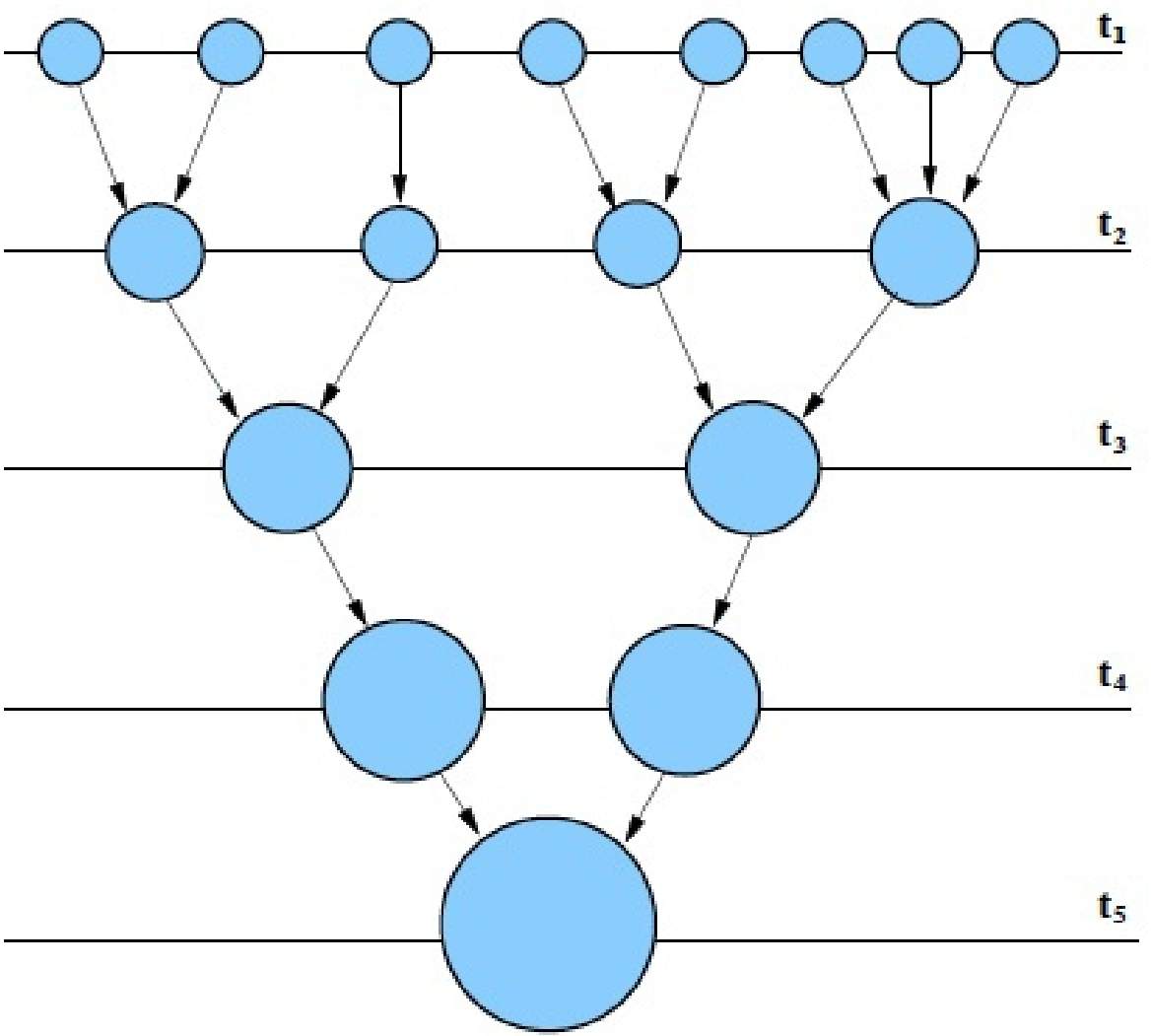

Merger tree incorporating subhalos

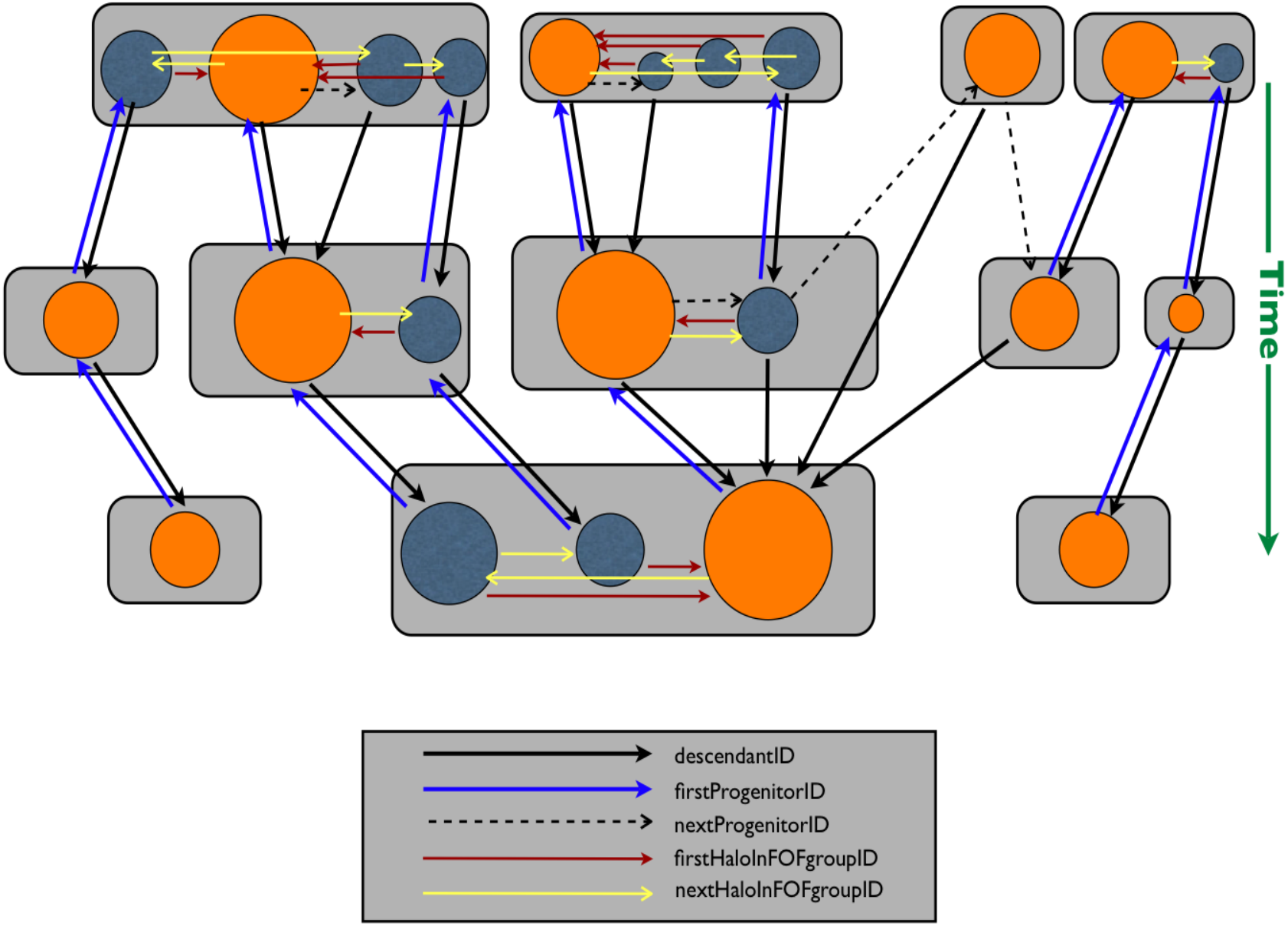

The most-massive self-bound subhalo in a FOF group is referred to as its main subhalo (sometimes the main halo) and usually contains most of its mass. Other subhaloes of the FOF group are referred to as satellite subhaloes. After implementation of the galaxy formation model, each FOF group hosts a 'central galaxy', which sits at the potential minimum of the main subhalo. Other associated galaxies may sit at the potential minima of smaller subhaloes or may no longer correspond to a resolved DM substructure ('orphans'). These galaxies are collectively referred to as satellites.

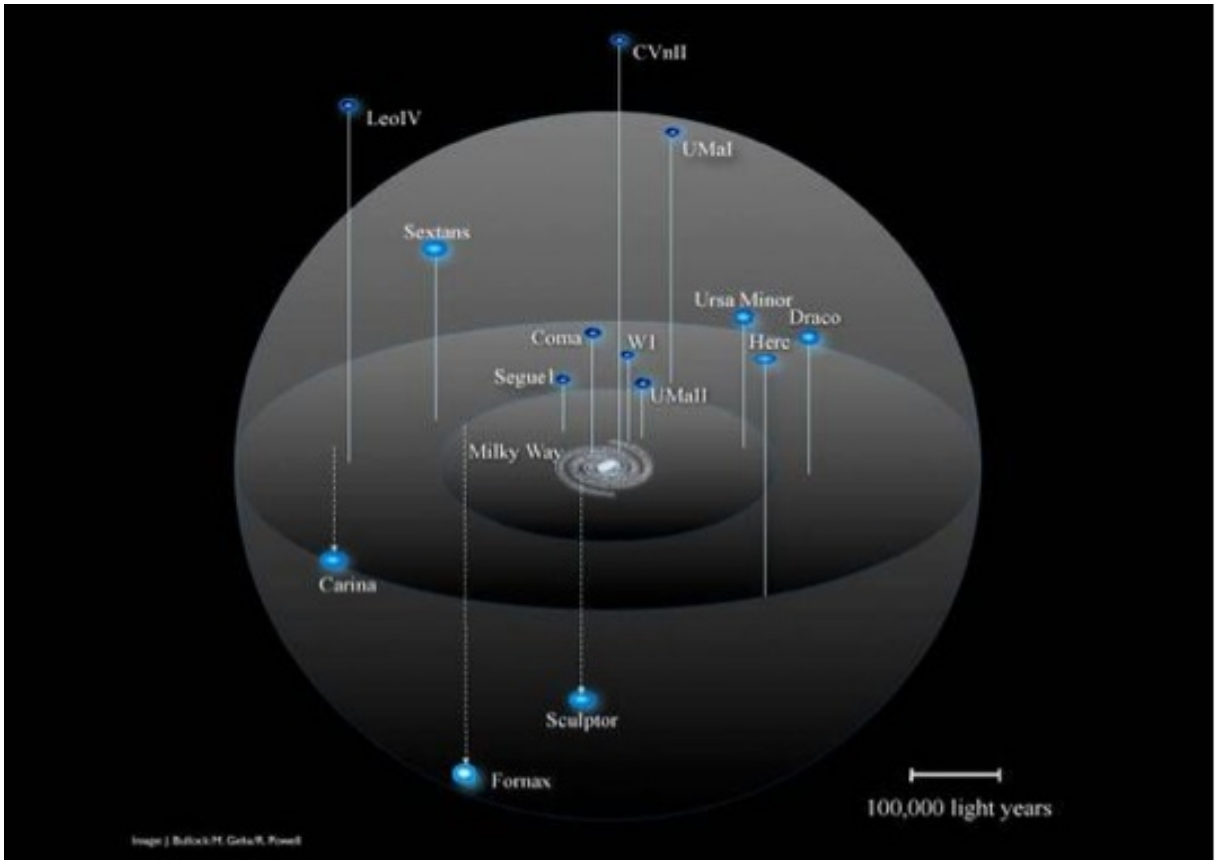

We define the centre of a FOF group to be its potential minimum and its virial radius to be the radius of the largest sphere with this centre and a mean overdensity exceeding 200 times the critical value. The total mass within the virial radius is defined as the virial mass of the group. Virial radius and virial mass are then related by

$$R_{\rm vir} = \left[\frac{G}{100}\frac{M_{\rm vir}}{H^2(z)}\right]^{1/3}.$$

The baryonic content of galaxies is split into five components, a stellar bulge, a stellar disc, a gas disc, a hot gas halo and an ejecta reservoir. These components exchange material through a variety of processes and their total mass grows through accretion from the IGM.

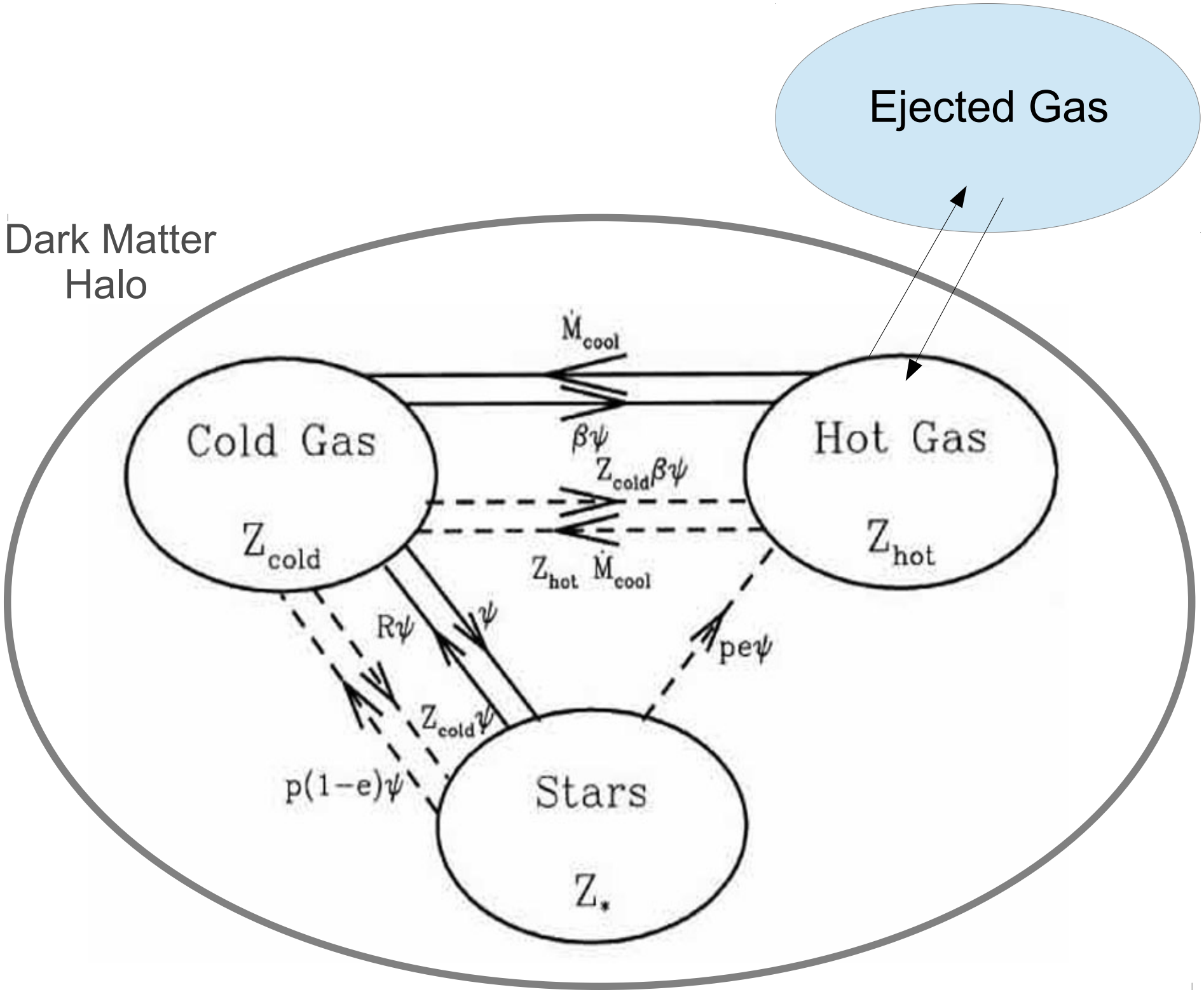
Ejected Gas
Dark Matter Halo
$\dot{M}_{cool}$
Cold Gas
Z_{cold}
$\beta\psi$
$Z_{cold}\beta\psi$
Hot Gas
Z_{hot}
$Z_{hot}\ \dot{M}_{cool}$
$R\psi$
ψ
$pe\psi$
$Z_{cold}\psi$
$p(1-e)\psi$
Stars
Z_*

Heating and Cooling Processes in Dark Matter Halos

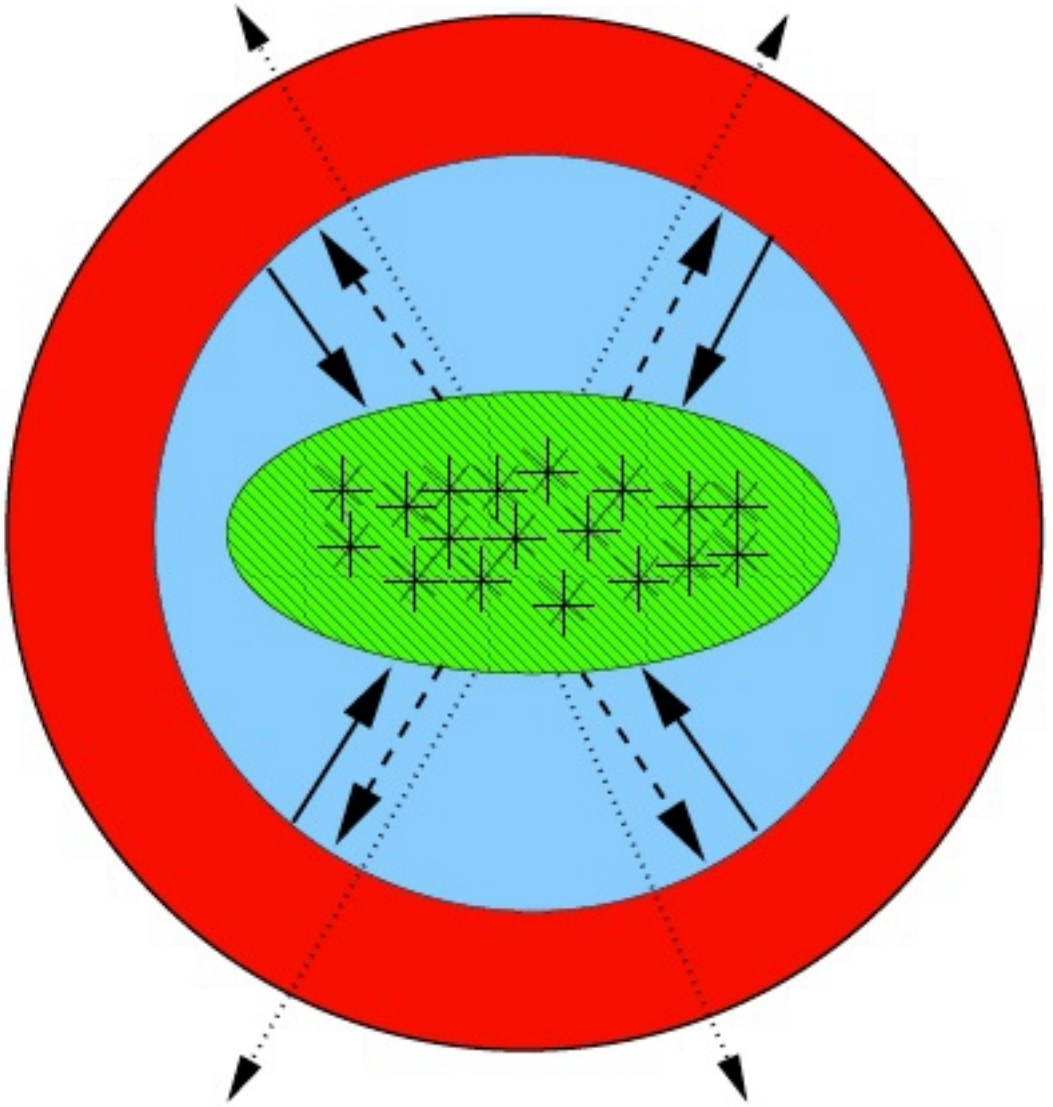

One mechanism which may contribute to the low efficiency of dwarf galaxy formation is photoheating of pre-galactic gas by the UV background. This inhibits gas condensation within DM haloes if the thermal energy exceeds the halo potential well depth.

In recent years, a number of simulations of this process have been carried out. Here we use a fitting function of the form originally proposed by Gnedin (2000) to describe how the baryon fraction in a halo depends on mass and redshift:

$$f_{\rm b}(z, M_{\rm vir}) = f_{\rm b}^{\rm cos}\left(1 + \left(2^{\alpha/3} - 1\right)\left[\frac{M_{\rm vir}}{M_{\rm F}(z)}\right]^{-\alpha}\right)^{-3/\alpha}. \qquad (2)$$

In this formula, $f_{\rm b}^{\rm cos} = 17$ per cent is the universal baryon fraction as given by first-year *WMAP* estimates (Spergel et al. 2003) and $\alpha = 2$ is a fit to the simulations in Okamoto et al. (2008). $M_{\rm F}$ is the characteristic halo mass of this 'filter'. In haloes with $M_{\rm vir} \gg M_{\rm F}(z)$, the baryon fraction is set to the universal value, while in haloes with $M_{\rm vir} \ll M_{\rm F}(z)$, it drops as $(M_{\rm vir}/M_{\rm F})^3$. The redshift dependence of $M_{\rm F}$ is determined by the details of how the reionization process occurred. Here, we use a table of $M_{\rm F}(z)$ kindly provided by Okamoto et al. (2008) from their simulations; $M_{\rm F}$ varies from $\sim 6.5 \times 10^9\,{\rm M}_\odot$ at $z = 0$ to $\sim 10^7\,{\rm M}_\odot$ just after reionization at $z \sim 8$.

Following cooling model in White & Frenk 1991:

infalling gas is shock-heated to the virial temperature of the host halo at an accretion shock and that its distribution interior to this shock is a quasi-static isothermal sphere with density falling as the inverse square of radius. The cooling time at each radius can then be calculated as

$$t_{\rm cool}(r) = \frac{3\mu m_{\rm H} k T_{\rm vir}}{2\rho_{\rm hot}(r)\Lambda(T_{\rm hot}, Z_{\rm hot})}, \quad (3)$$

where $\mu m_{\rm H}$ is the mean particle mass, k is the Boltzmann constant, $\rho_{\rm hot}(r)$ is the hot gas density at radius r, $\Lambda(T_{\rm hot}, Z_{\rm hot})$ is the temperature- and metallicity-dependent cooling functions (Sutherland & Dopita 1993), and $Z_{\rm hot}$ is the metallicity of the hot halo gas. $T_{\rm hot} = 35.9(V_{\rm vir}/{\rm km\,s^{-1}})^2\,{\rm K}$ is the assumed virial temperature of the host halo. For main subhaloes, the gas temperature is updated according to the current circular velocity at the virial radius at each snapshot, while for satellite subhaloes, we assume the gas temperature to be constant at the value it had when the subhalo was accreted on to its main halo.

The cooling radius is then estimated through

$$r_{\rm cool} = \left[\frac{t_{\rm dyn,h} m_{\rm hot} \Lambda(T_{\rm hot}, Z_{\rm hot})}{6\pi\mu m_{\rm H} k T_{\rm vir} R_{\rm vir}}\right]^{1/2}. \quad (4)$$

The definition of the halo dynamical time, $t_{\rm dyn,h}$, involves an arbitrary constant. Here we adopt the convention $t_{\rm dyn,h} \equiv R_{\rm vir}/V_{\rm vir} = 0.1H(z)^{-1}$ as in De Lucia, Kauffmann & White (2004). Readers are referred to Croton et al. (2006) and Somerville et al. (2008) for the discussion of other possible choices of $t_{\rm dyn,h}$ when defining $r_{\rm cool}$. When $r_{\rm cool} < R_{\rm vir}$, we assume that we are indeed in the cooling flow regime and that the cooling rate on to the central galaxy is[1]

$$\dot{M}_{\rm cool} = m_{\rm hot} \frac{r_{\rm cool}}{R_{\rm vir}} \frac{1}{t_{\rm dyn,h}}. \tag{5}$$

Conversely, when $r_{\rm cool} > R_{\rm vir}$, we assume that we are in the rapid infall regime and gas accretes on to the central object in free-fall; thus, on the halo dynamical time

$$\dot{M}_{\rm cool} = \frac{m_{\rm hot}}{t_{\rm dyn,h}}. \tag{6}$$

Star Formation

$SFR = M_{gas} / t_{dyn}$; $t_{dyn} = \lambda R_{vir} / V_c$

(Schmidt-Kennicutt type star formation prescription)

Feedback from Supernovae

. Here we assume that SN feedback injects gas from the cold disc into the hot halo and, in addition, can transfer halo gas to the ejecta reservoir.

We estimate the amount of cold disc gas that is reheated by SN feedback and injected into the hot halo component as

$$\delta M_{\rm reheat} = \epsilon_{\rm disc} \times \delta M_*. \qquad (18)$$

where δM_* is the mass of newly formed long-lived stars. DLB07 took $\epsilon_{\rm disc}$ to be a constant, based on some observational indications that mass outflow rates are typically a few times the SFR in actively star-forming galaxies.

$$\epsilon_{\rm disc} = \epsilon \times \left[0.5 + \left(\frac{V_{\rm max}}{70\,{\rm km\,s^{-1}}}\right)^{-\beta_1}\right], \quad (19)$$

where ϵ and β_1 are free parameters describing the ratio of reheated mass to new stellar mass in massive galaxies and the scaling of this ratio with $V_{\rm max}$ in dwarfs, respectively. The circular velocity dependence is motivated by the fact that less energy is needed to heat a solar mass of gas to the halo virial temperature and to eject it from the disc in lower mass galaxies. A naive argument leads to the expectation $\beta_1 \sim 2$, but a variety of factors could lead to a different dependence, so we adjust both β_1 and ϵ when fitting to observations, in particular to the observed stellar mass function.

We parametrize the total amount of energy effectively injected by massive stars into disc and halo gas as

$$\delta E_{\rm SN} = \epsilon_{\rm halo} \times \frac{1}{2} \delta M_* V_{\rm SN}^2, \tag{20}$$

where $0.5V_{\rm SN}^2$ is the mean kinetic energy of SN ejecta per unit mass of stars formed and, following Croton et al. (2006), we take $V_{\rm SN} = 630\,{\rm km\,s^{-1}}$, based on standard assumptions for the stellar IMF and the energetics of SN explosions. In this case also, DLB07 assumed the efficiency $\epsilon_{\rm halo}$ to be a constant. However, since dwarf galaxies have stronger winds, lower metallicities and less dust than galaxies like our own, it is plausible that radiative losses during the thermalization of ejecta energy are substantially smaller in dwarfs than in giants. We have therefore allowed for this possibility explicitly by setting

$$\epsilon_{\rm halo} = \eta \times \left[0.5 + \left(\frac{V_{\rm max}}{70\,{\rm km\,s^{-1}}} \right)^{-\beta_2} \right], \tag{21}$$

where η is a free parameter which encodes possible variations about our IMF and SN assumptions, possible energy input from the winds and UV radiation of massive stars, and the radiative losses during ejecta thermalization, while β_2 describes the dependence of this last factor on $V_{\rm max}$. Again, we adjust these parameters when fitting to observations of the stellar mass function and gas-to-star ratios of

Given this energy input into disc and halo gas, the total amount of material that can ejected from a halo/subhalo can be estimated as

$$\delta M_{\rm ejec} = \frac{\delta E_{\rm SN} - \frac{1}{2}\delta M_{\rm reheat} V_{\rm vir}^2}{\frac{1}{2} V_{\rm vir}^2}. \quad (22)$$

If this equation gives $\delta M_{\rm ejec} < 0$, we assume that the mass of reheated gas saturates at $\delta M_{\rm reheat} = \delta E_{\rm SN}/(\frac{1}{2} V_{\rm vir}^2)$ and that no gas is ejected from the halo/subhalo.

The gas mass, $M_{\rm ejec}$, thrown out of a system by these effects is stored in an ejecta 'reservoir' associated with the halo/subhalo, whence it may later be reincorporated into the hot halo gas and so again become available for cooling on to the central galaxy. In low-mass haloes, hot winds are likely to leave at a substantially higher velocity relative to the escape velocity and so their gas is likely to be more difficult to reaccrete. To allow for this possibility, we introduce a dependence of the reaccretion rate on halo/subhalo virial velocity:

$$\dot{M}_{\rm ejec} = -\gamma \left(\frac{V_{\rm vir}}{220\,{\rm km\,s^{-1}}} \right) \left(\frac{M_{\rm ejec}}{t_{\rm dyn,h}} \right), \quad (23)$$

where γ is a free parameter which we take to be 0.3.

Black hole growth: "quasar" mode

The quasar mode applies to black hole growth during gas-rich mergers. During a merger, the central black hole of the major progenitor grows both by absorbing the central black hole of the minor progenitor and by accreting cold gas. The total growth in mass is calculated as

$$\delta M_{\rm BH} = M_{\rm BH,min} + f\left(\frac{M_{\rm min}}{M_{\rm maj}}\right)\left[\frac{M_{\rm cold}}{1+(280\,{\rm km\,s^{-1}})/V_{\rm vir}}\right], \qquad (36)$$

where $M_{\rm BH,min}$ is the mass of the black hole in the minor progenitor, $M_{\rm cold}$ is the total cold gas in the two progenitors, and $M_{\rm min}$ and $M_{\rm maj}$ are the total baryon masses of the minor and major progenitors, respectively. Here f is a free parameter, which, following Croton et al. (2006), we set to 0.03 in order to reproduce the observed local $M_{\rm BH}$–$M_{\rm bulge}$ relation. Both major mergers and gas-rich minor mergers contribute significantly to the growth of the black hole. We do not explicitly model feedback due to this mode, which always coincides with a starburst in the merging galaxies.

Black hole growth: "radio" mode

Radio mode growth occurs through hot gas accretion on to central black holes. The growth rate in this mode is calculated, following Croton et al. (2006), as

$$\dot{M}_{\rm BH} = \kappa \left(\frac{f_{\rm hot}}{0.1}\right) \left(\frac{V_{\rm vir}}{200\,{\rm km\,s^{-1}}}\right)^3 \left(\frac{M_{\rm BH}}{10^8\,h^{-1}\,{\rm M}_\odot}\right) {\rm M}_\odot\,{\rm yr}^{-1}, \quad (37)$$

where, for a main subhalo, the hot gas fraction, $f_{\rm hot}$, is the ratio of hot gas mass, $M_{\rm hot}$, to subhalo DM mass, $M_{\rm DM}$, while for a type 1 galaxy in a satellite subhalo, $f_{\rm hot}$ is the ratio of hot gas mass to DM mass within $R_{\rm strip}$, $\frac{R_{\rm strip}}{R_{\rm DM,infall}} M_{\rm DM,infall}$. The parameter κ sets the efficiency of hot gas accretion. Again following Croton et al. (2006), we assume that this hot-mode accretion deposits energy in relativistic jets with 10 per cent efficiency and that this energy is then deposited as heat in the hot gas atmosphere.

Table 1. Summary of those parameters of our preferred model which were adjusted primarily to fit the observed $z = 0$ stellar mass function.

Parameter	Description	Preferred value
α	Star formation efficiency (Section 3.4)	0.02
ϵ	Amplitude of SN-reheating efficiency (Section 3.5)	6.5
β_1	Slope of SN-reheating efficiency (Section 3.5)	3.5
η	Amplitude of SN-ejection efficiency (Section 3.5)	0.32
β_2	Slope of SN-ejection efficiency (Section 3.5)	3.5
γ	Ejecta reincorporation efficiency (Section 3.5)	0.3
κ	Hot gas accretion efficiency on to black holes (Section 3.9)	1.5×10^{-5}

Effect of feedback on the Luminosity Function

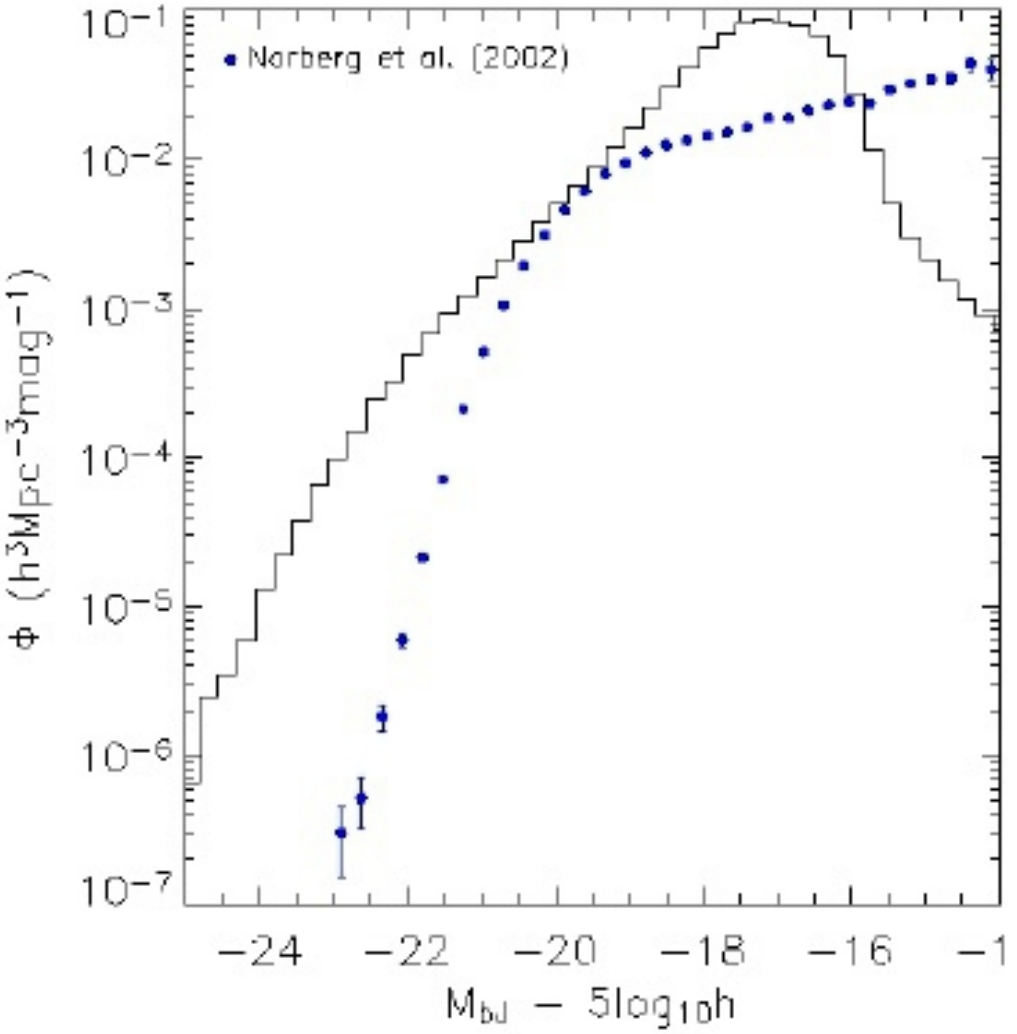

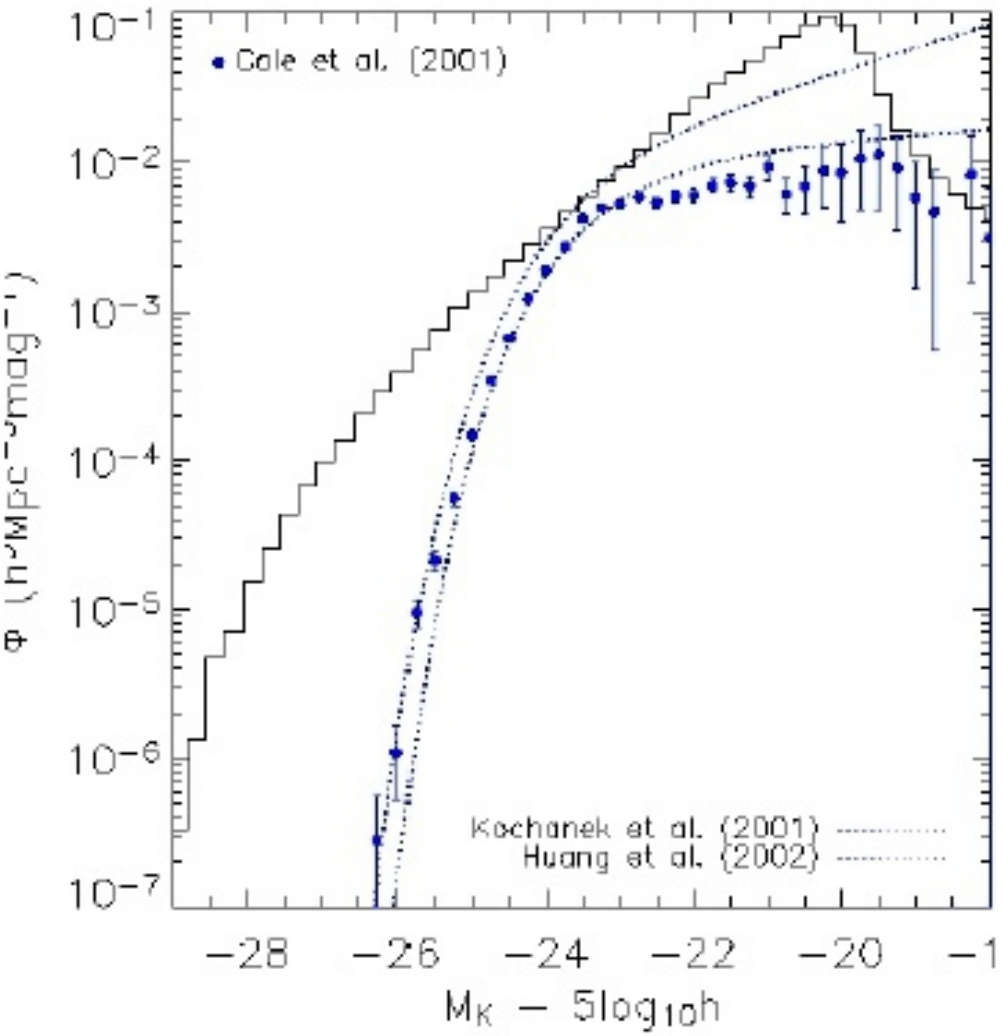

Full model with ~~reionisation~~, ~~AGN~~ and ~~SN~~ feedback

Croton et al 2006

Effect of feedback on the Luminosity Function

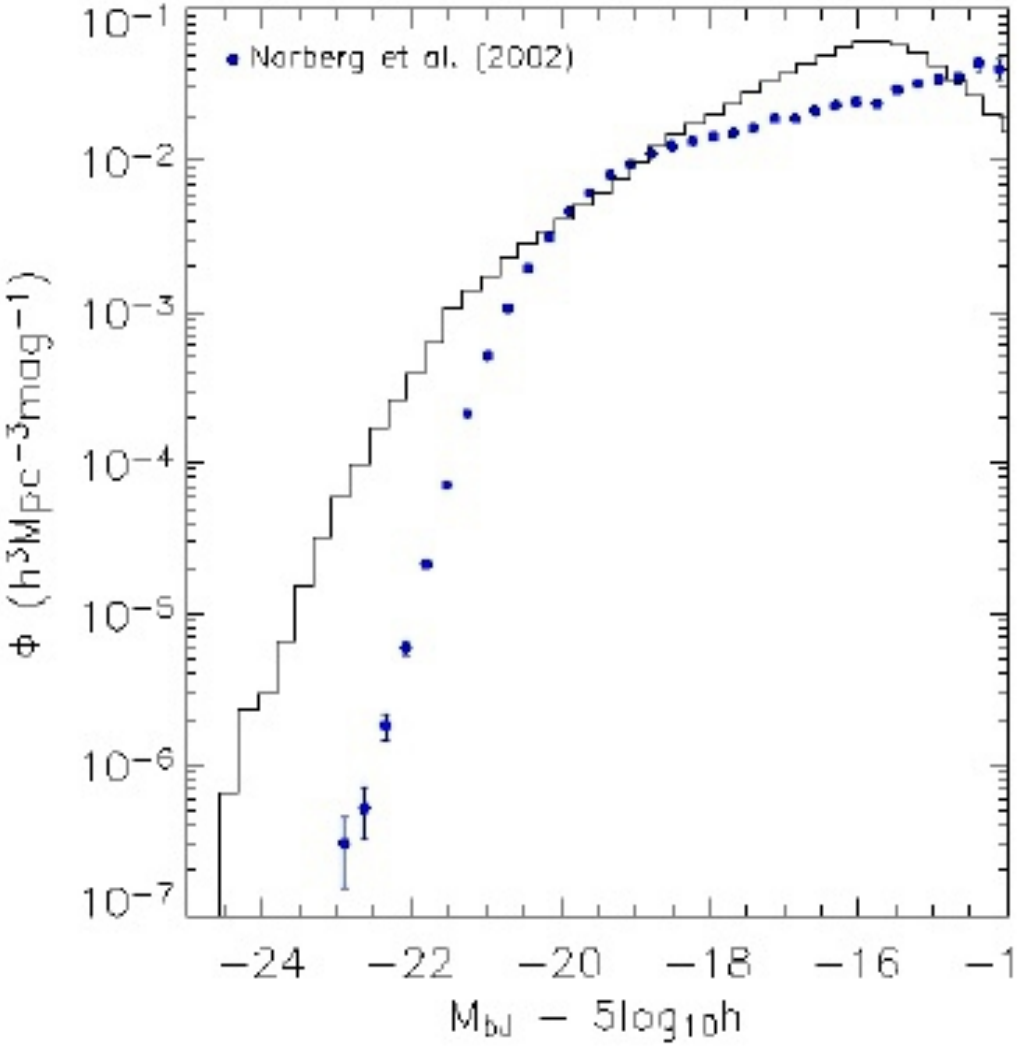

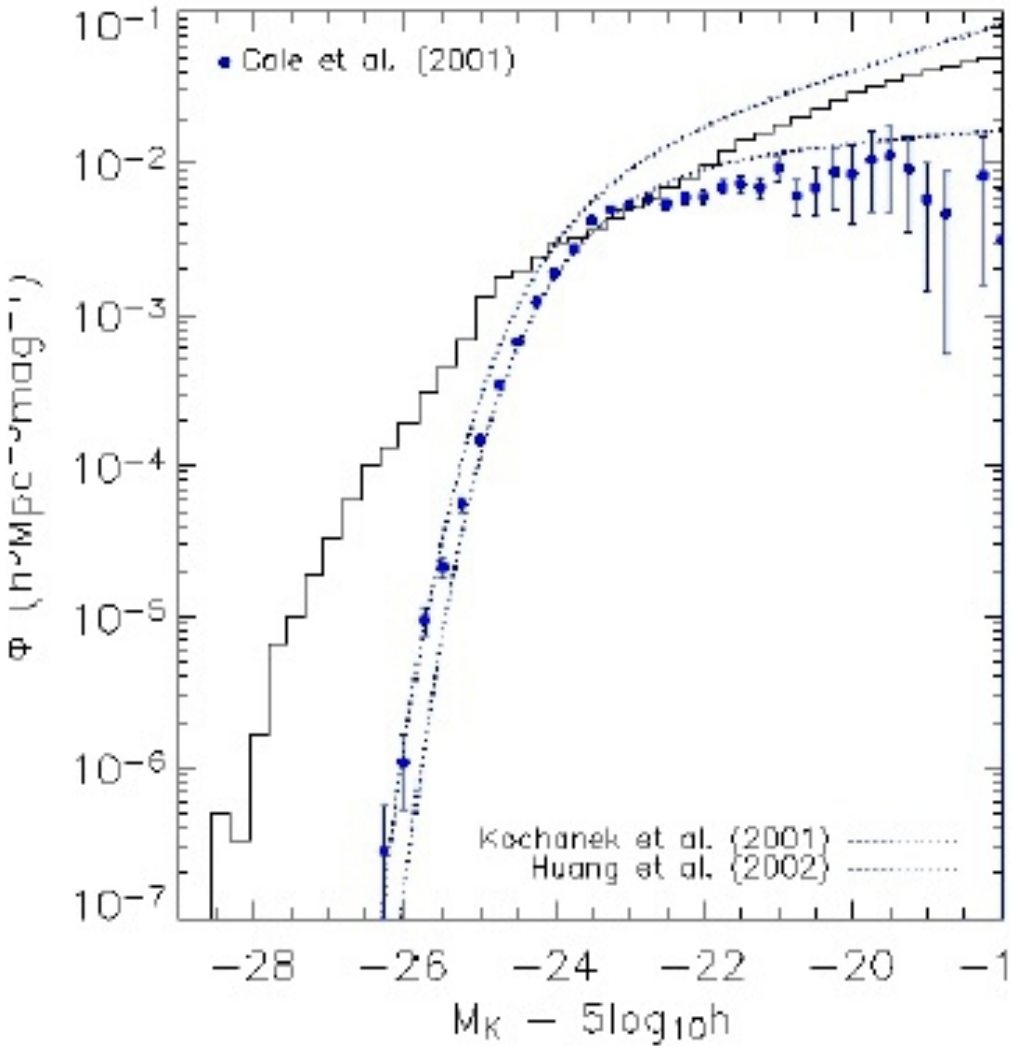

Full model with ~~reionisation~~, ~~AGN~~ and SN feedback Croton et al 2006

Effect of feedback on the Luminosity Function

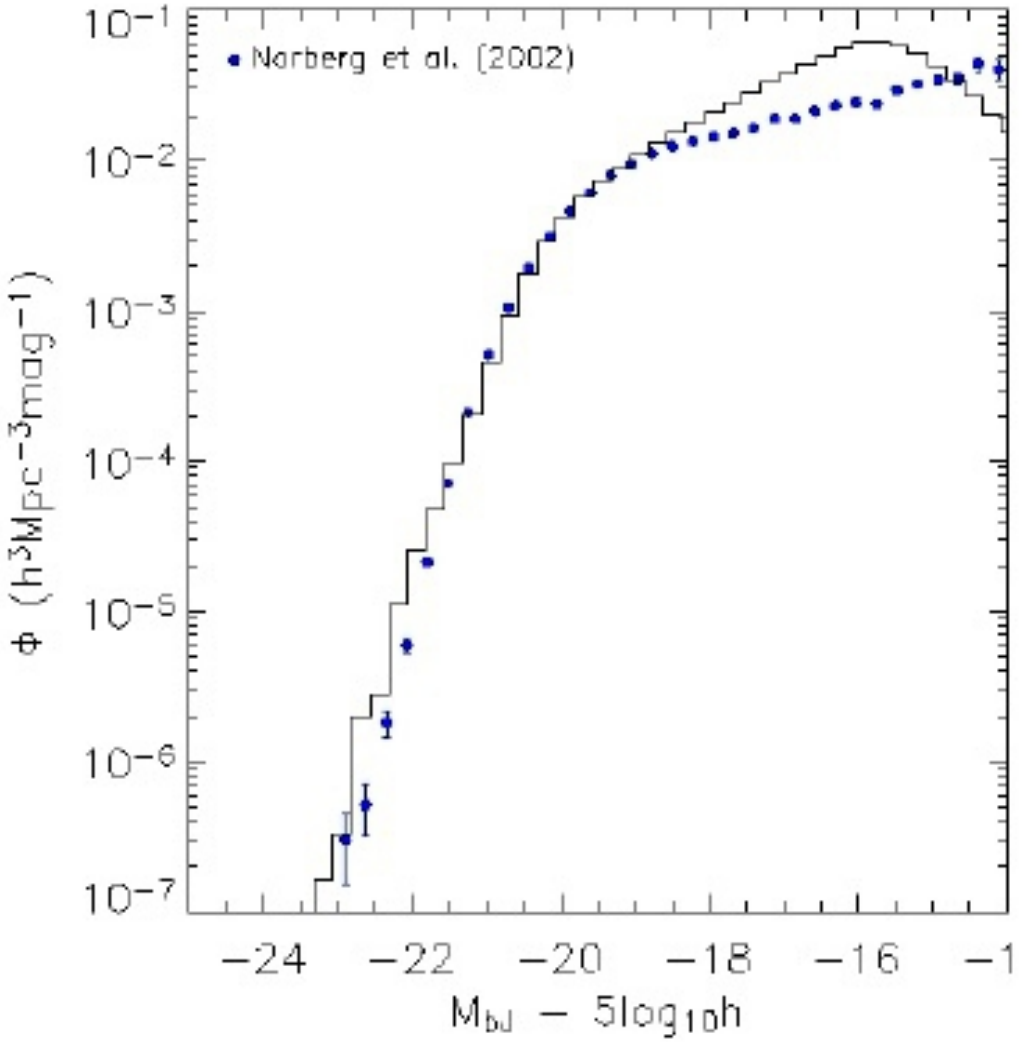

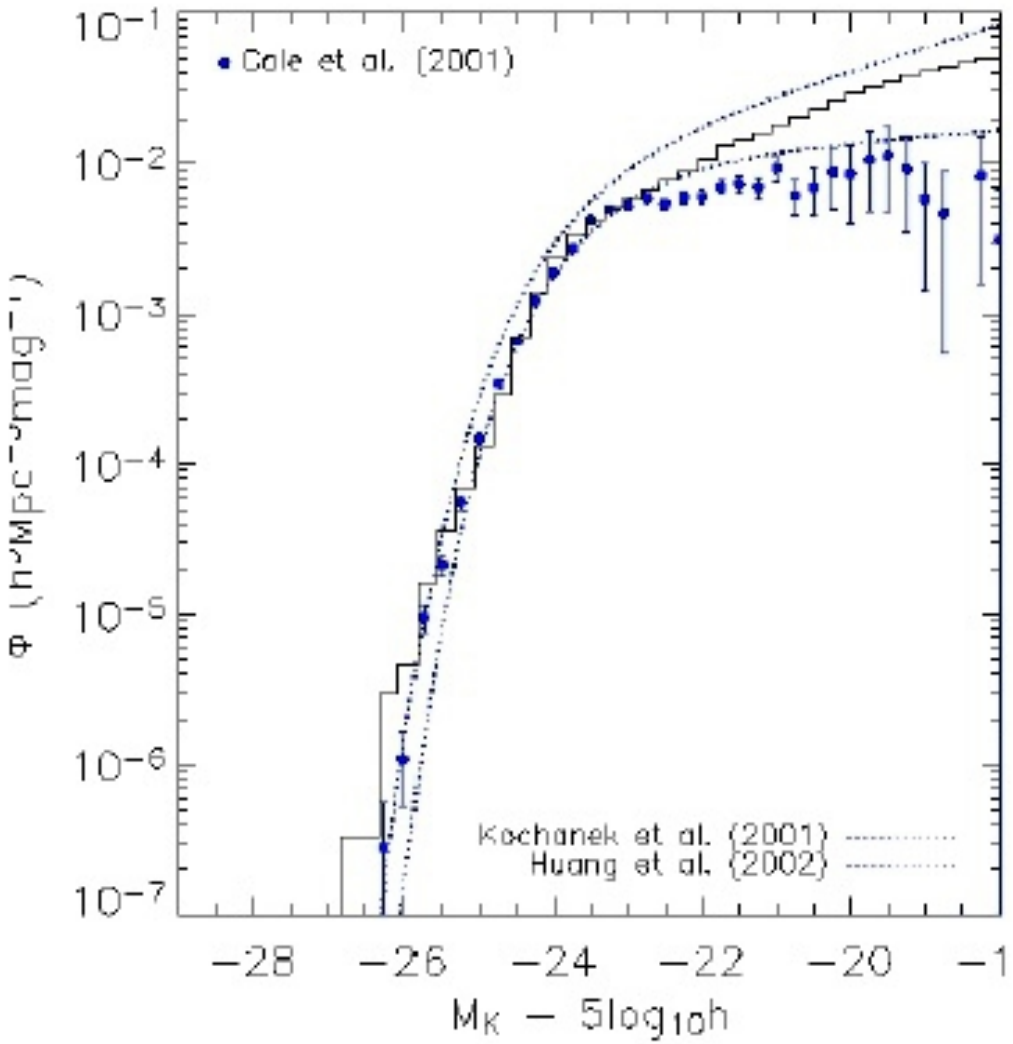

Full model with ~~reionisation~~, AGN and SN feedback Croton et al 2006

Effect of feedback on the Luminosity Function

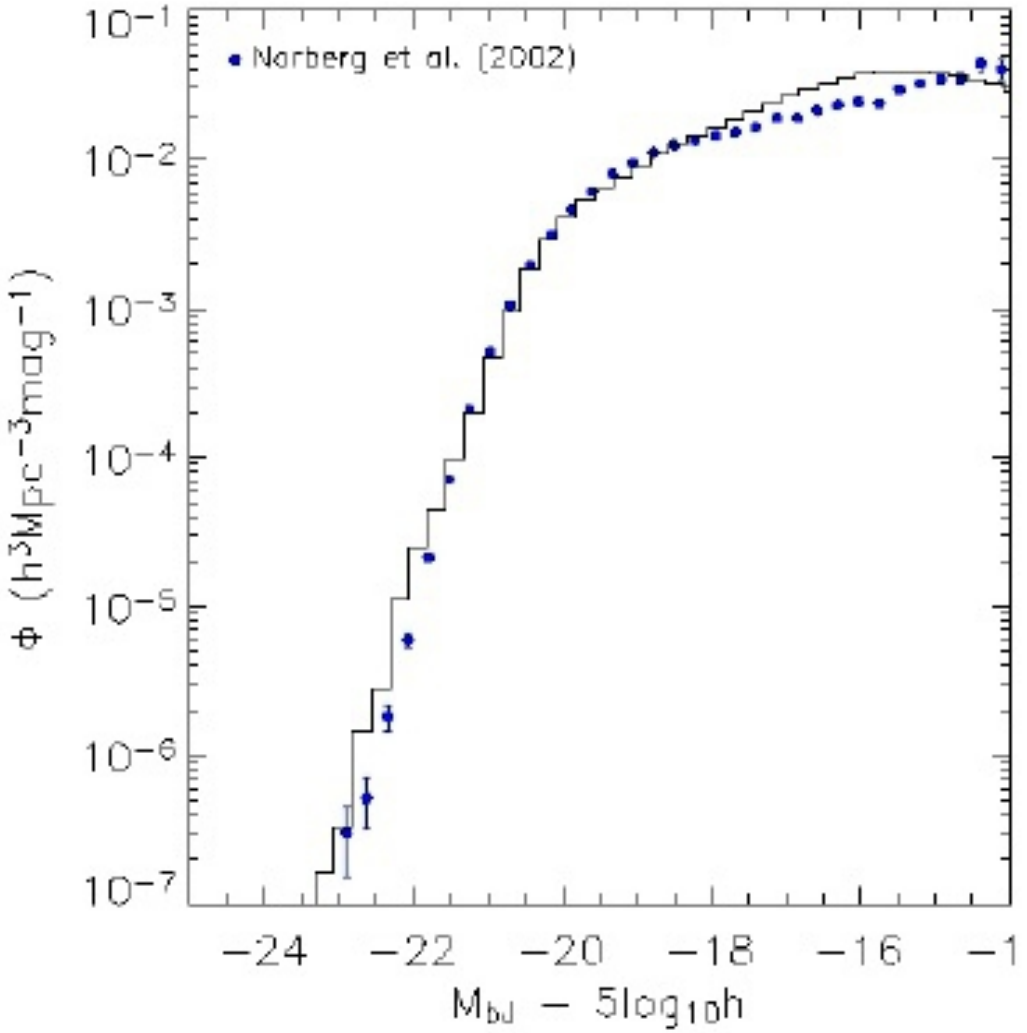

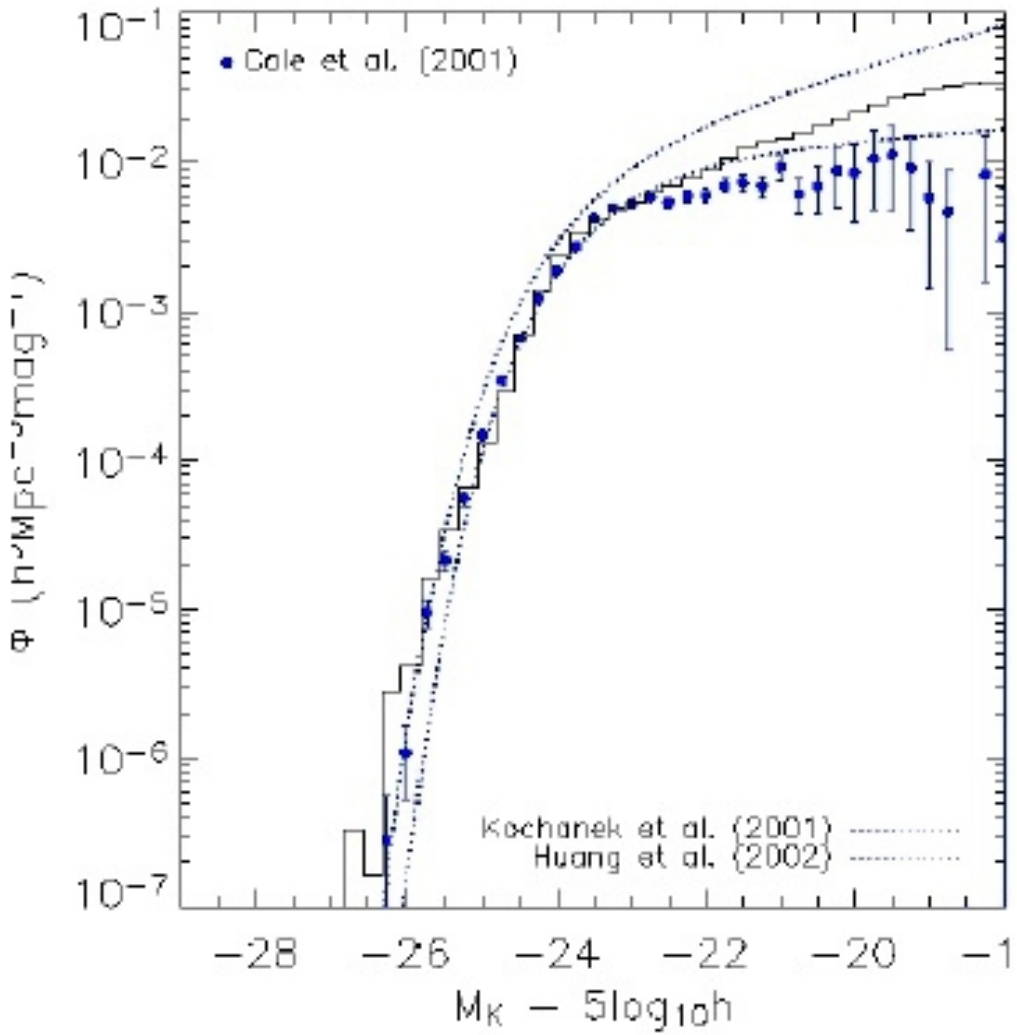

Full model with reionisation, AGN and SN feedback Croton et al 2006

Firefox

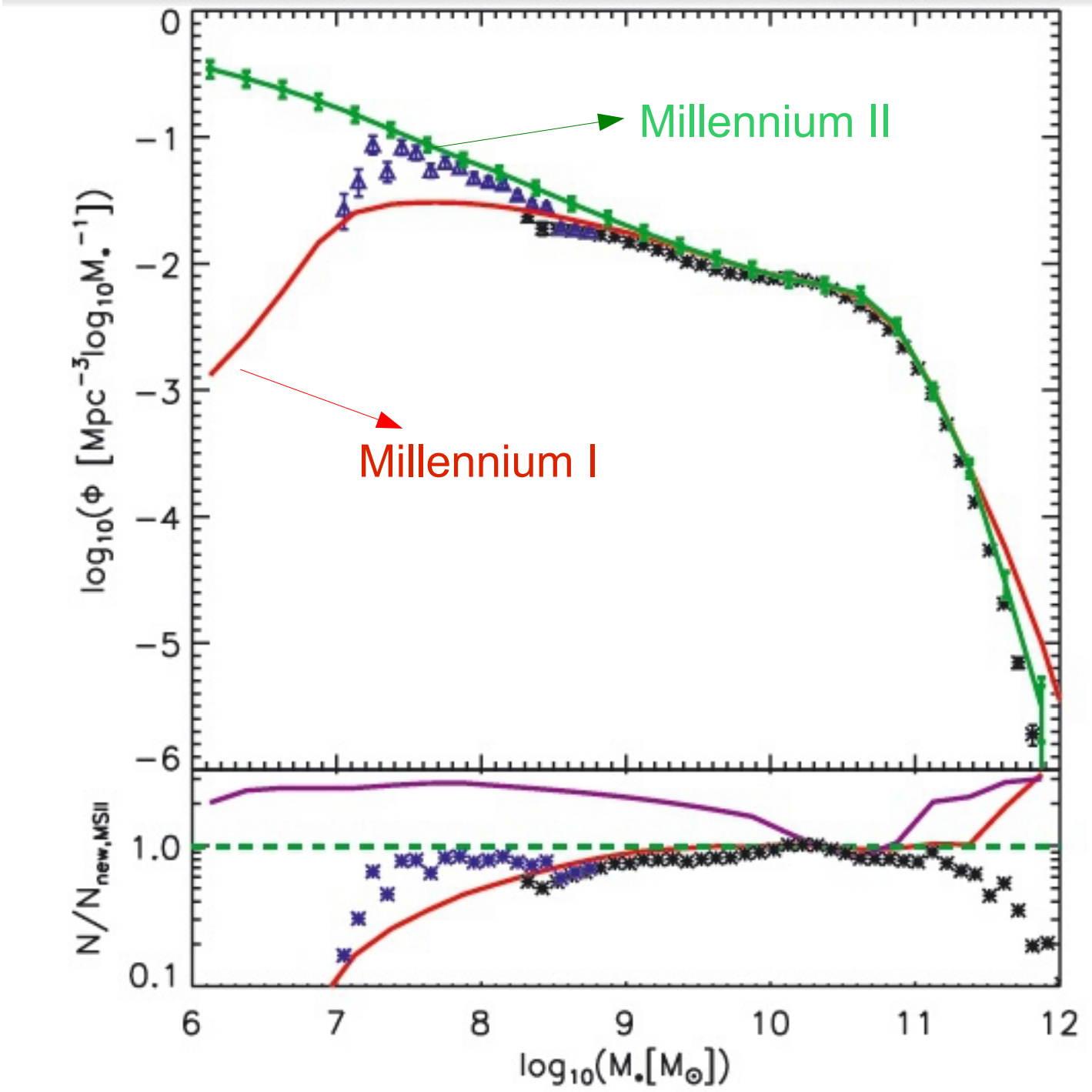

Figure 7. The abundance of galaxies as a function of their stellar mass.

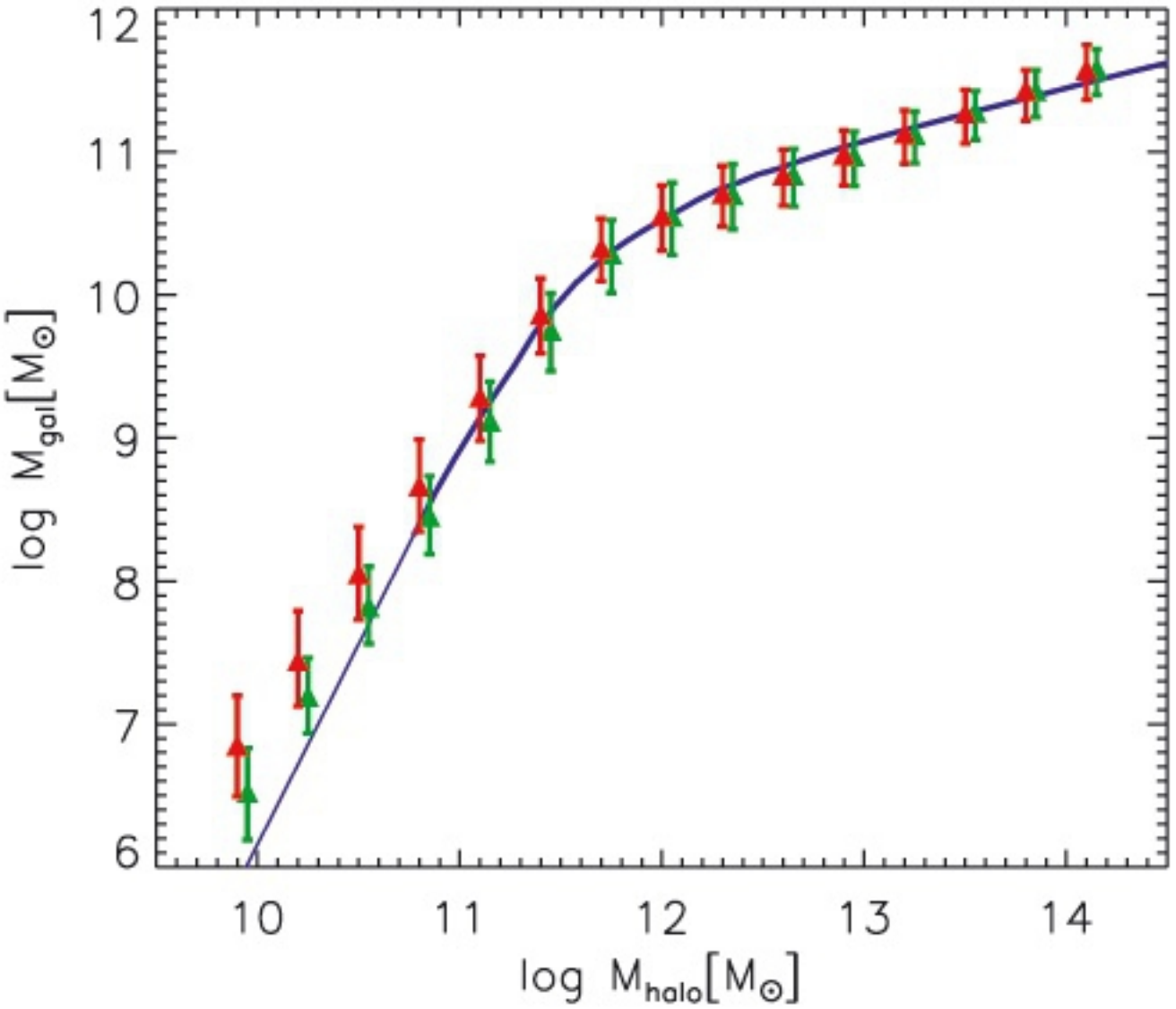

Figure 9. Galaxy stellar mass as a function of the maximum past halo mass.

OBSERVABLE: The Tully-Fisher Relation linking galaxy luminosity/mass to the peak circular velocity

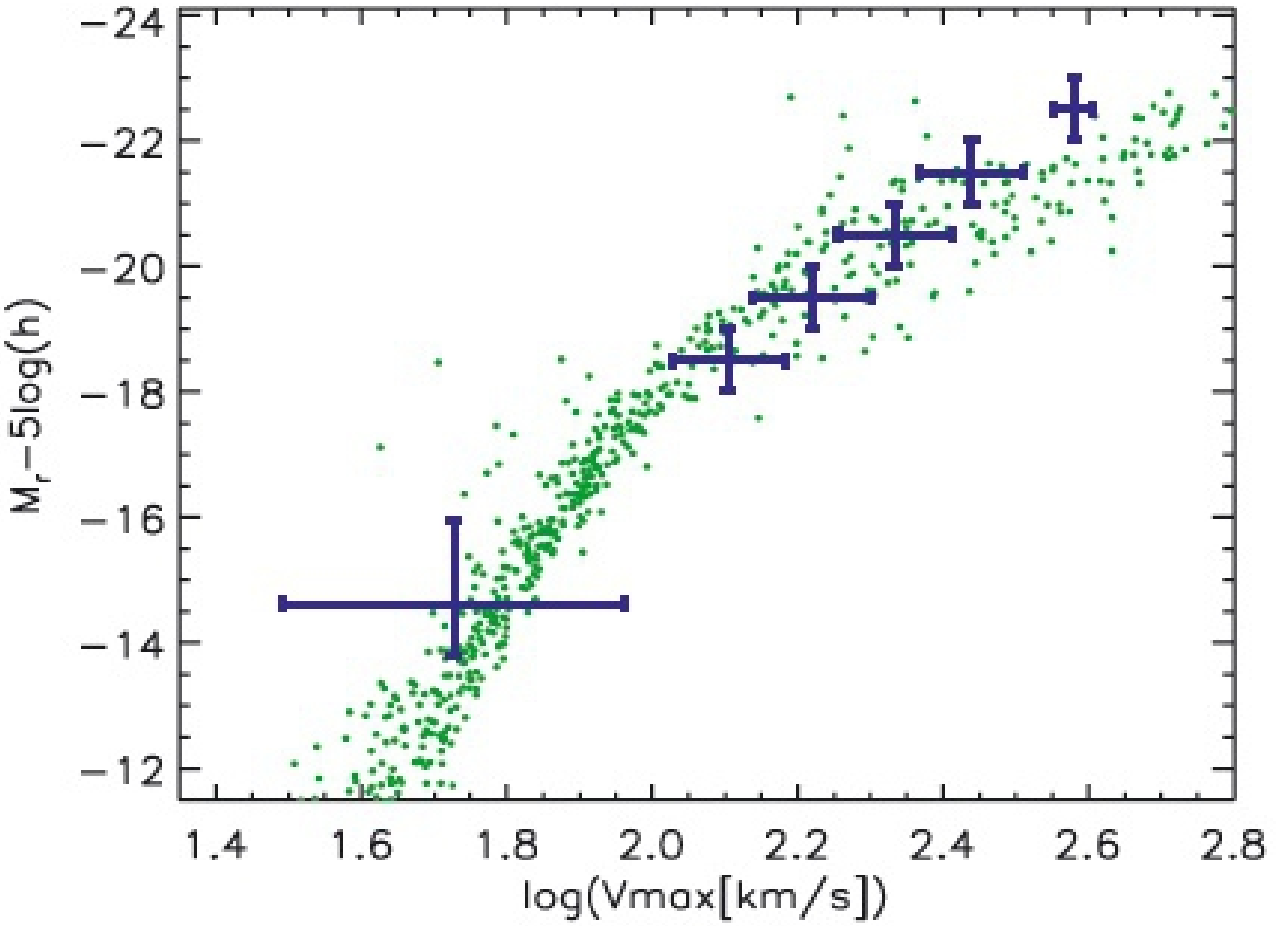

Figure 13. *r*-band TF relation. Blue symbols with error bars are observational results for isolated disc galaxies taken from Blanton, Geha & West (2008) and from Springob et al. (2007).

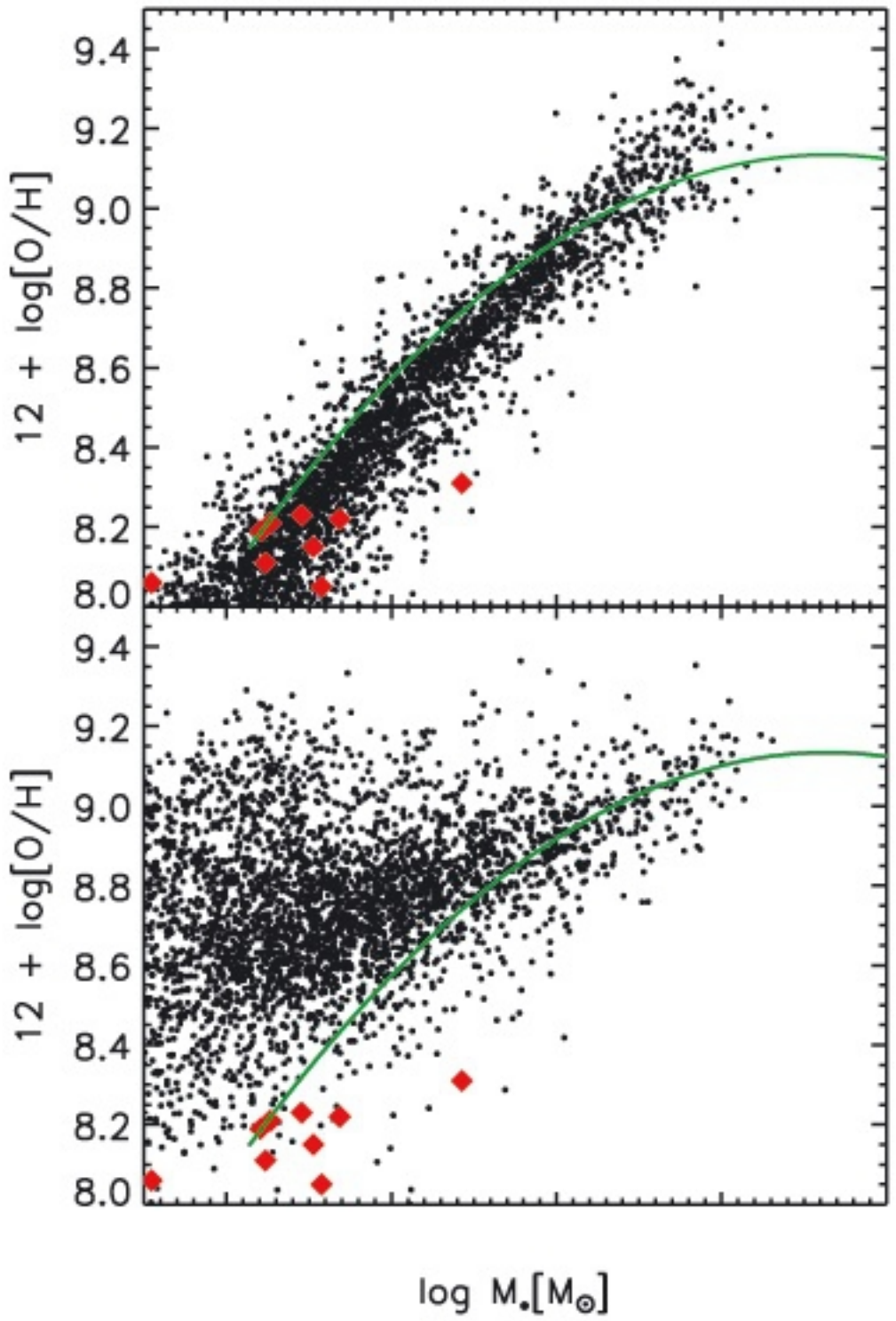

MASS-METALLICITY RELATION

LUMINOSITY FUNCTION OF MILKY WAY SATELLITES

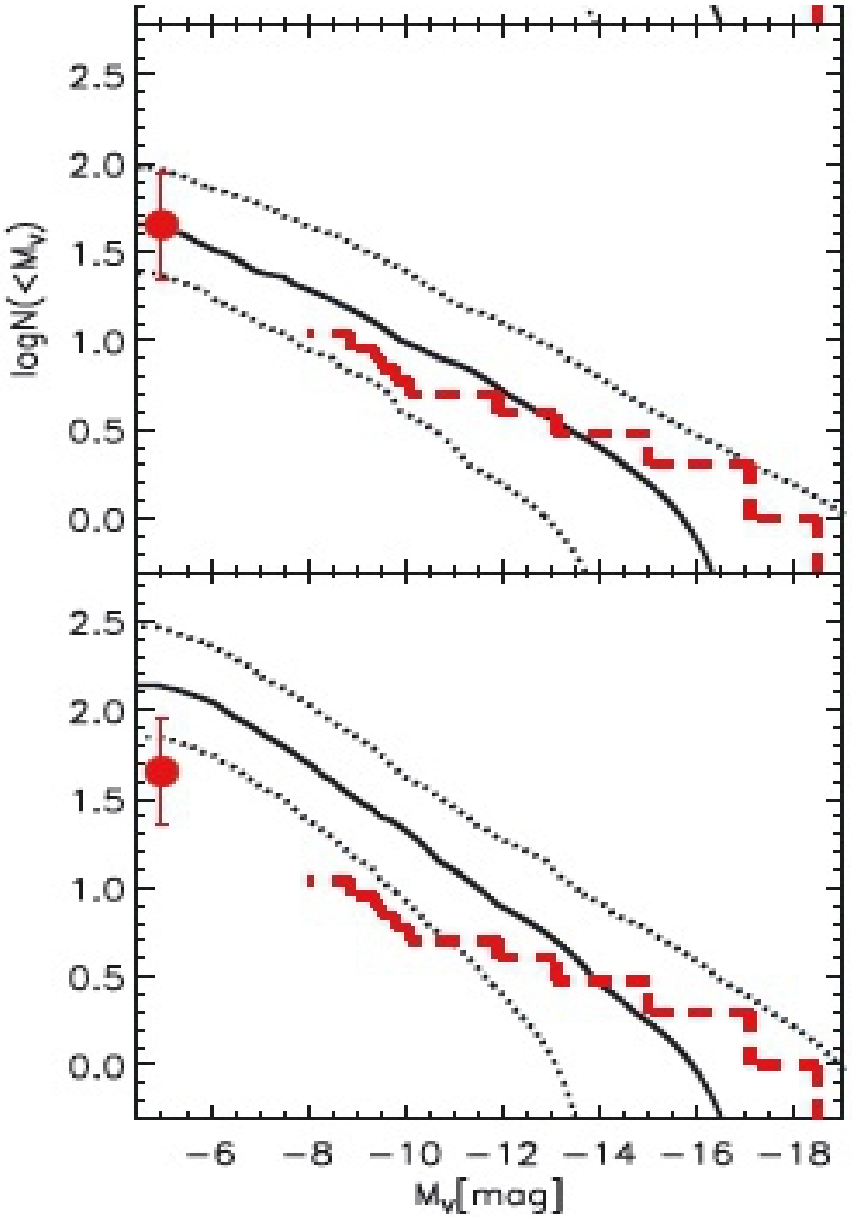

With photo-ionization heating

Without photo-ionization heating

BIMODALITY?

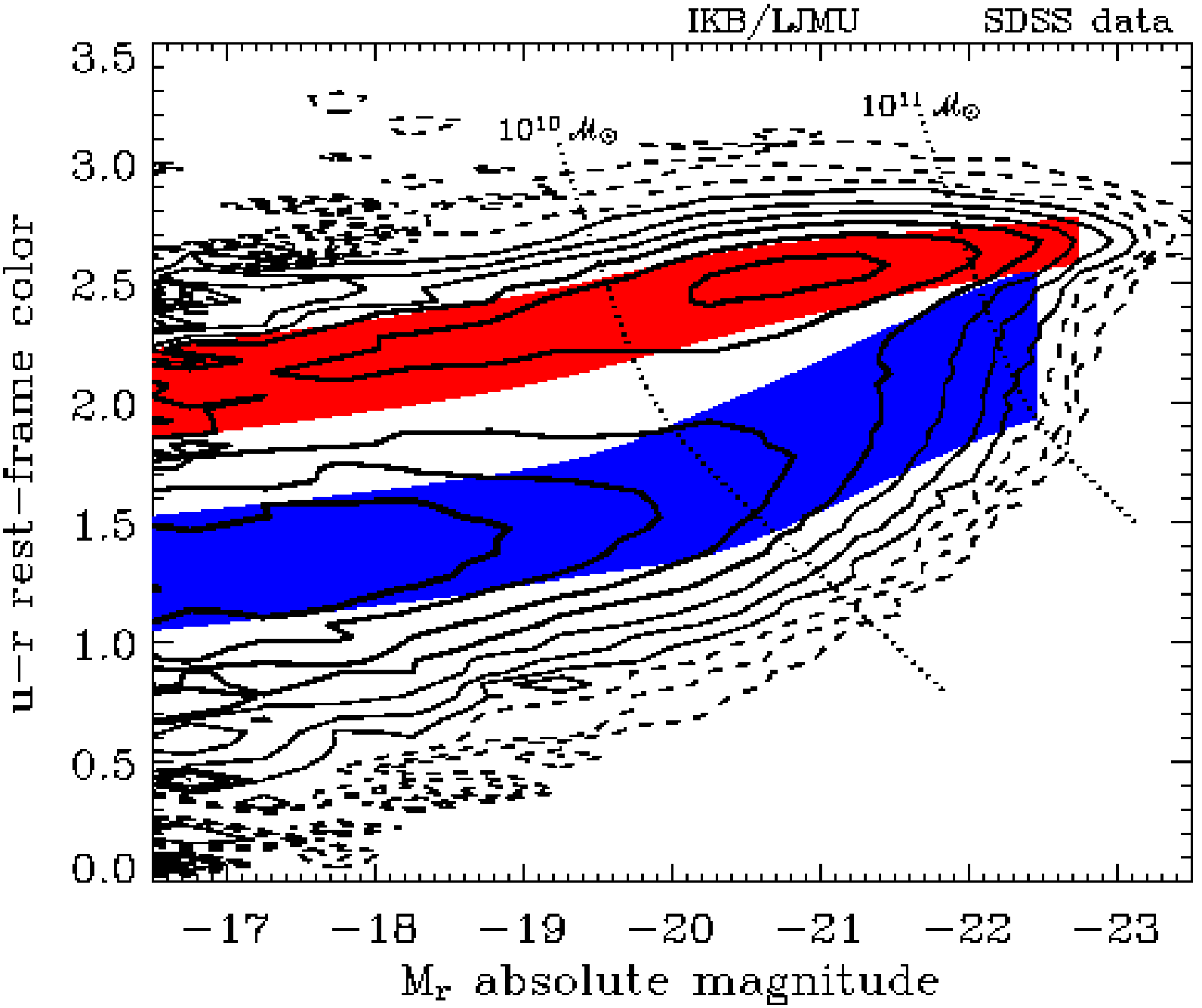
IKB/LJMU
SDSS data
$10^{10}\,M_\odot$
$10^{11}\,M_\odot$
u−r rest−frame color
3.5
3.0
2.5
2.0
1.5
1.0
0.5
0.0
−17
−18
−19
−20
−21
−22
−23
M_r absolute magnitude

Colour distributions in the models

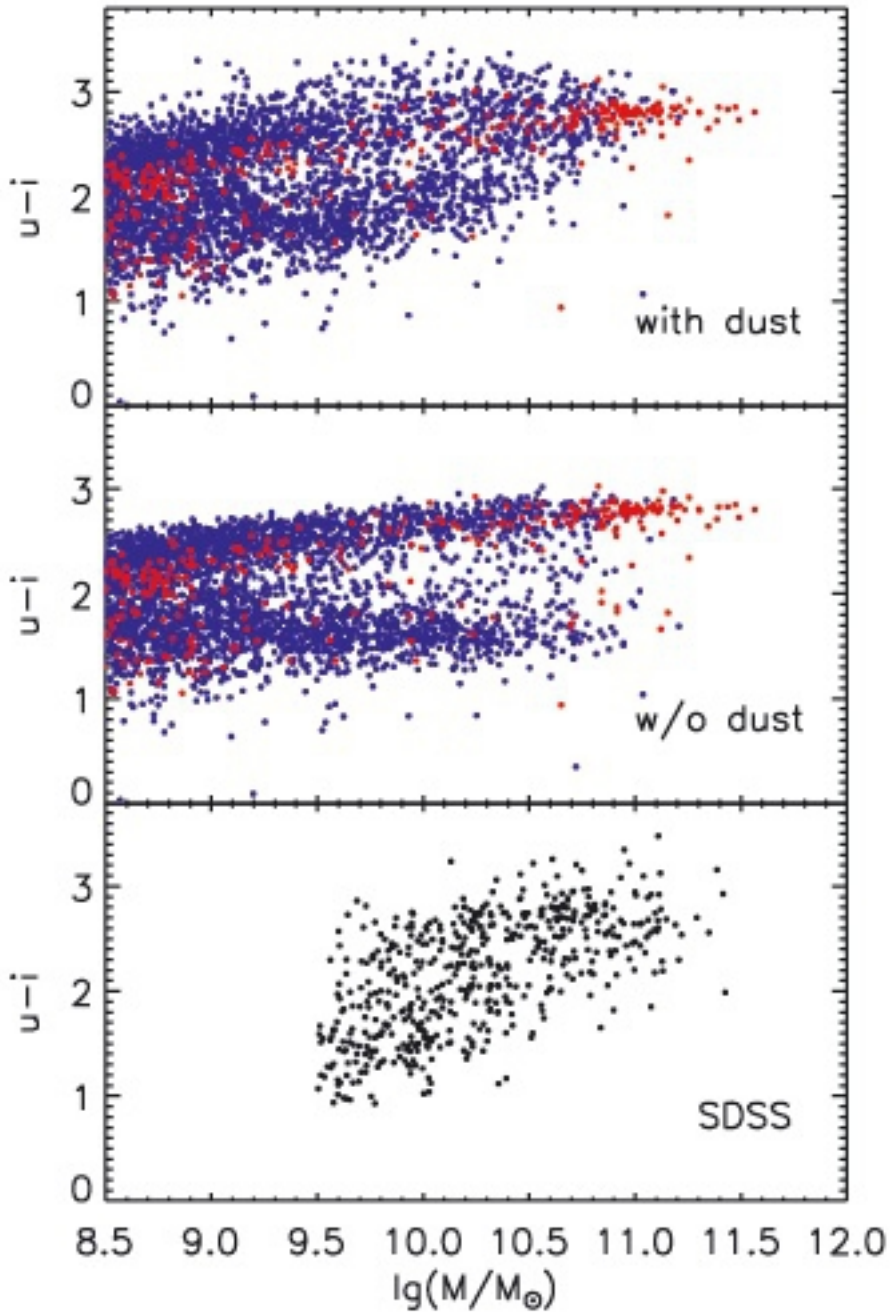

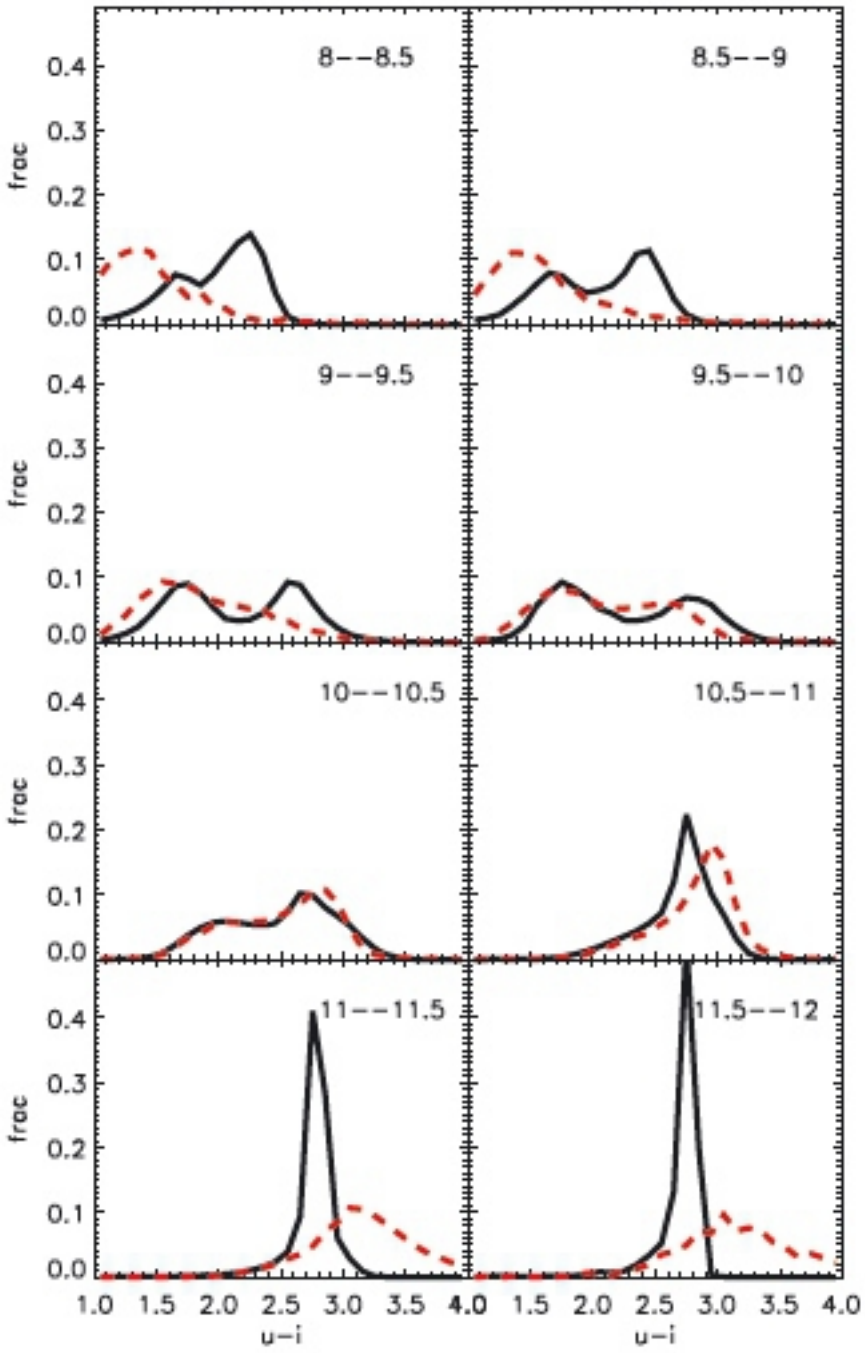

Figure 12. $u - i$ colour distributions as a function of stellar mass. Solid

Two-point correlation function in bins of stellar mass

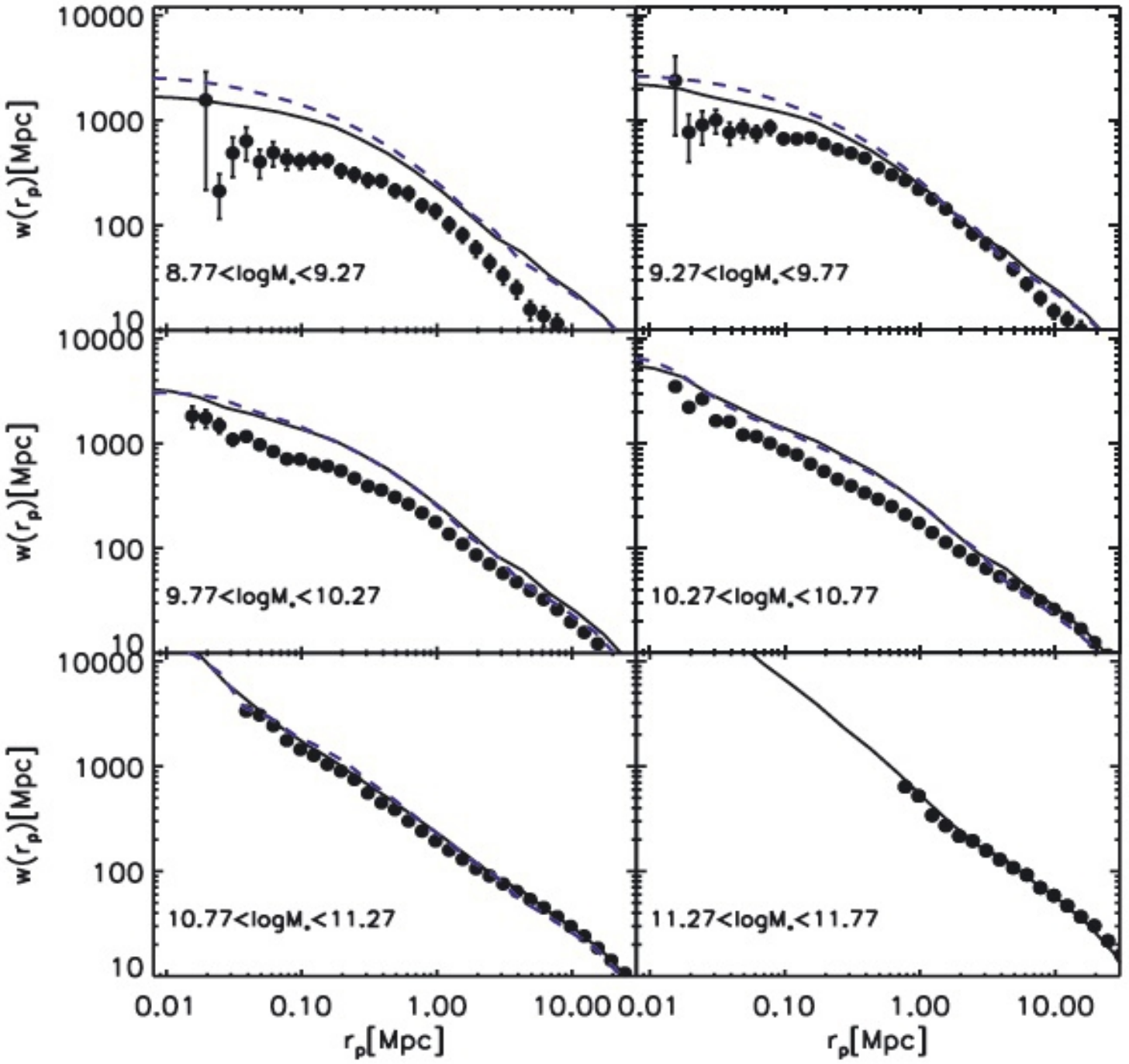

PROCESSES ACTING ON SATELLITE GALAXIES

We assume the hot gas in a subhalo to have a distribution that exactly parallels that of the DM. Since tidal acceleration acts identically on hot gas and DM at each location, we take the hot gas mass to be reduced by tidal stripping in direct proportion to the subhalo's DM mass. The latter is, of course, followed explicitly in a dynamically consistent way by the original simulation. Thus, we assume

$$\frac{M_{\rm hot}(R_{\rm tidal})}{M_{\rm hot,infall}} = \frac{M_{\rm DM}}{M_{\rm DM,infall}}, \tag{24}$$

where $M_{\rm DM,infall}$ and $M_{\rm hot,infall}$ were the DM mass of the subhalo and the mass of its associated hot gas, when its central galaxy was last a type 0 galaxy, and $M_{\rm DM}$ and $M_{\rm hot}$ are the current masses of these two components, respectively. Recall that we assume $\rho \propto r^{-2}$ for the hot gas distribution; thus, $M_{\rm hot}(r) \propto r$. The tidal radius beyond which the hot gas is stripped can be thus expressed as

$$R_{\rm tidal} = \left(\frac{M_{\rm DM}}{M_{\rm DM,infall}}\right) R_{\rm DM,infall}, \tag{25}$$

where $R_{\rm DM,infall}$ was the virial radius of the subhalo just before it became a satellite.

In addition to tidal forces, the hot gas around satellite galaxies experiences ram-pressure forces due to the satellite's motion through the intracluster medium. At a certain distance, $R_{\rm r.p.}$, from the centre of the satellite, self-gravity is approximately balanced by this ram pressure:

$$\rho_{\rm sat}(R_{\rm r.p.})V_{\rm sat}^2 = \rho_{\rm par}(R)V_{\rm orbit}^2, \tag{26}$$

where $\rho_{\rm sat}(R_{\rm r.p.})$ is the hot gas density of the satellite at radius $R_{\rm r.p.}$, $V_{\rm sat}$ is the virial velocity of the subhalo at infall (which we assume to be constant as the subhalo orbits around the main halo), $\rho_{\rm par}(R)$ is the hot gas density of the parent DM halo at distance R from the centre of its potential well and $V_{\rm orbit}$ is the orbital velocity of the satellite, which we estimate as the virial circular velocity of the main halo. The ram pressure dominates over gravity beyond $R_{\rm r.p.}$ and hot gas at these radii is stripped.

We compare the two radii $R_{\rm tidal}$ and $R_{\rm r.p.}$ and define the minimum of the two as the stripping radius

$$R_{\rm strip} = \min(R_{\rm tidal}, R_{\rm r.p.}). \tag{27}$$

Beyond $R_{\rm strip}$, we assume all the hot gas to be removed without modifying the gas profile within $R_{\rm strip}$.

We thus assume that the stellar component of a satellite galaxy is affected by tidal forces only after its subhalo has been entirely disrupted, that is, it has become a type 2 galaxy. The position of such a galaxy is identified with that of the most-bound particle of its subhalo at the last time the subhalo could be identified. To estimate when stripping of stars is important, we assume the satellite orbits in a singular isothermal potential

$$\phi(R) = V_{\rm vir}^2 \ln R. \tag{28}$$

Assuming conservation of energy and angular momentum along the orbit, its pericentric distance can be estimated from

$$\left(\frac{R}{R_{\rm peri}}\right)^2 = \frac{\ln R/R_{\rm peri} + (1/2)\,(V/V_{\rm vir})^2}{(1/2)\,(V_{\rm t}/V_{\rm vir})^2}, \tag{29}$$

where R is the current distance of the satellite from halo centre, and V and $V_{\rm t}$ are the velocity of the satellite galaxy with respect to the halo centre and its tangential part, respectively.

We compare the main halo density at the pericentre with the average baryon mass (cold gas mass + stellar mass) density of the satellite within its half-mass radius. If

$$\frac{M_{\rm DM,halo}(R_{\rm peri})}{R_{\rm peri}^3} \equiv \rho_{\rm DM,halo} > \rho_{\rm sat} \equiv \frac{M_{\rm sat}}{R_{\rm sat,half}^3}, \tag{30}$$

then we assume the satellite galaxy is disrupted entirely.

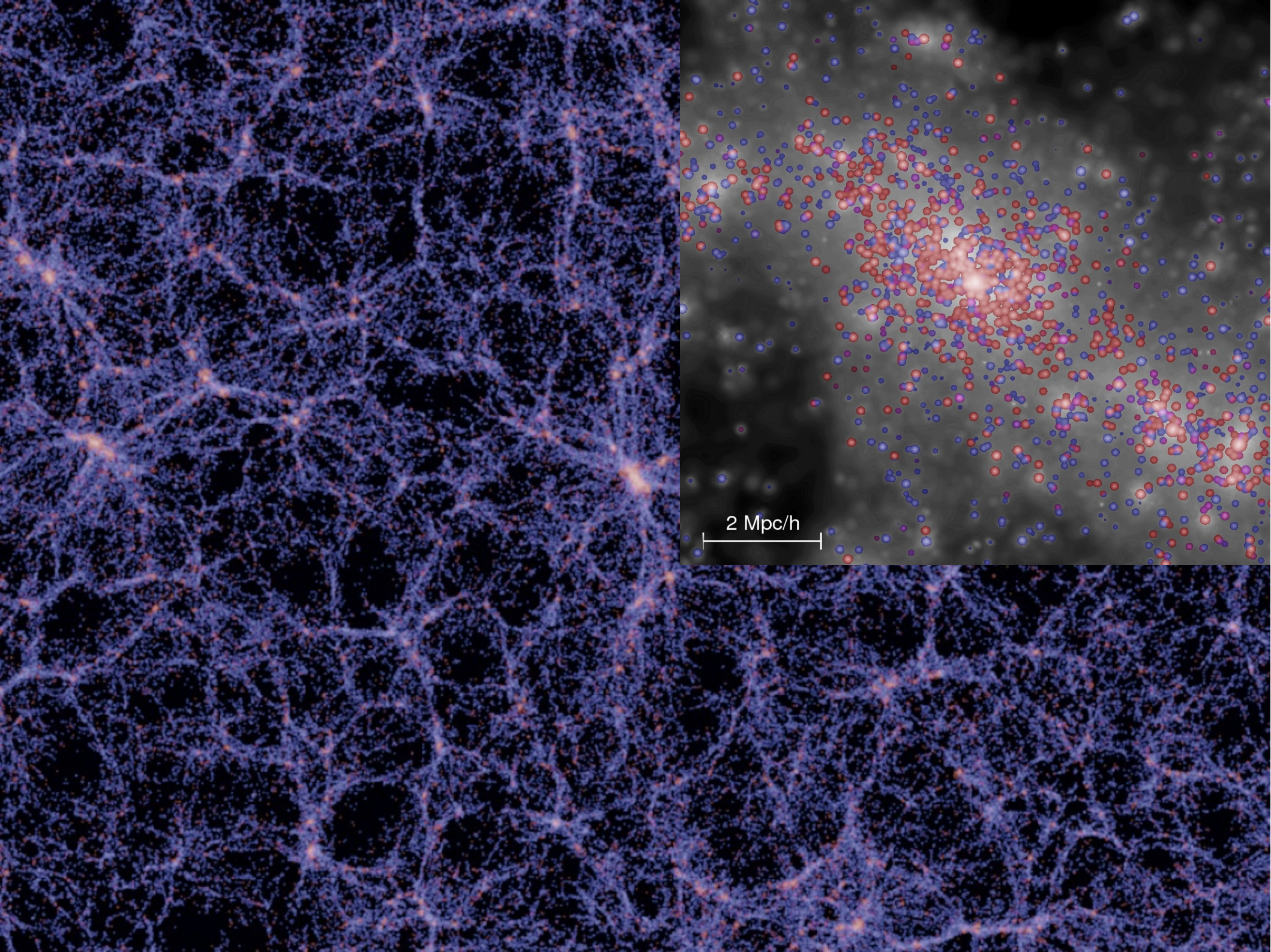
2 Mpc/h

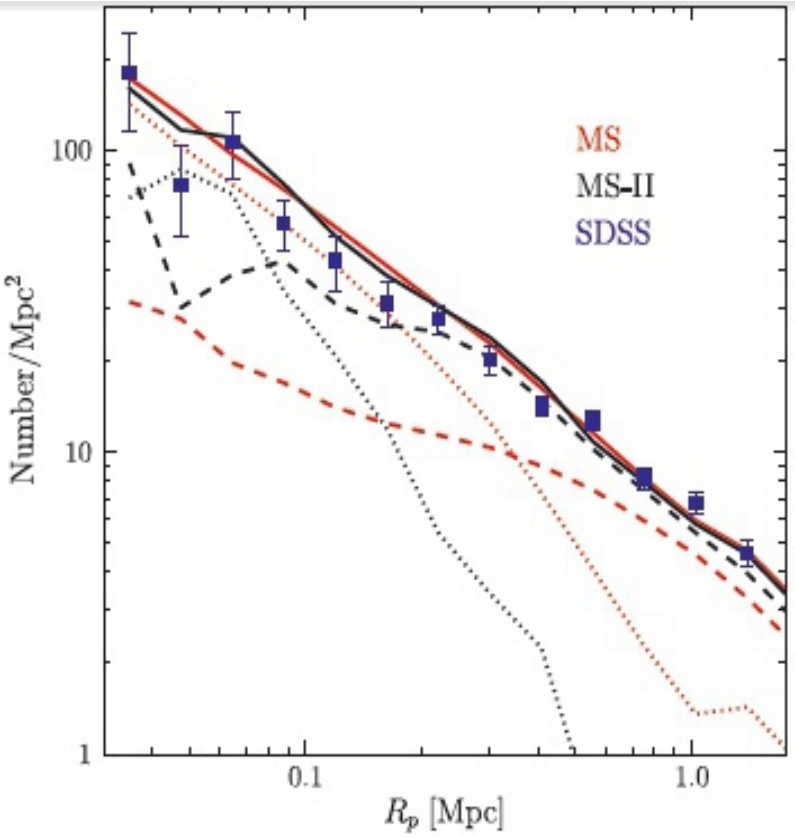

Figure 14. Projected galaxy number density profiles for samples of massive clusters from the MS (red lines), the MS-II (black lines) and the SDSS (blue symbols with error bars). Observational and model clusters are selected in the same way and are not scaled before stacking (see text for details). Solid lines are for all model galaxies with $M_* > 1.2 \times 10^{10}\,M_\odot$, while dashed and dotted lines split them into galaxies with surviving DM subhaloes and orphans, respectively. Note the excellent agreement in mean profile between the MS and the MS-II, despite the very different number of orphans in the two simulations. The SDSS profiles here have been corrected for the spectroscopic incompleteness of the survey, which varies as a function of the projected radius and reaches 60 per cent near the cluster centre. The error bars reflect the uncertainty in the mean estimated from the scatter among the 31 SDSS cluster profiles.

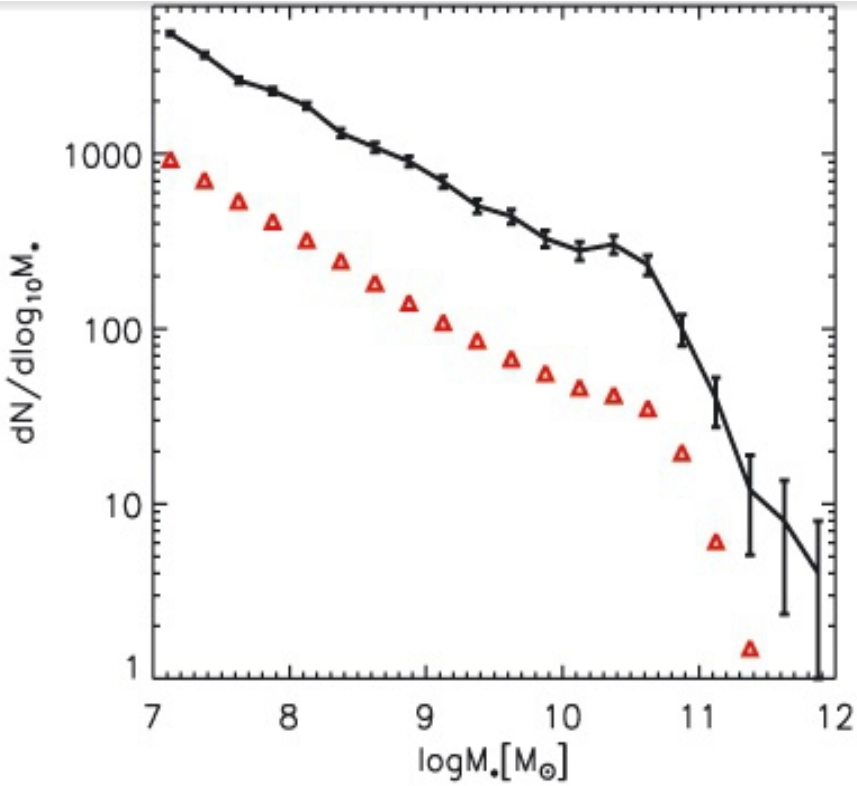

Figure 15. The stellar mass function of galaxies in a rich cluster. The solid curve links counts in 0.25-dex bins for galaxies within $R_{\rm vir} = 2$ Mpc of the centre of the most-massive cluster in the MS-II according to our preferred galaxy formation model. Error bars indicate Poisson uncertainties in these counts. Red open triangles represent the general stellar mass function of galaxies constructed from the MS-II as a whole. This has been renormalized arbitrarily to allow its shape to be compared to that of the cluster stellar mass function.

reflecting the fact that the passive galaxy fraction in general is somewhat too high in our model.

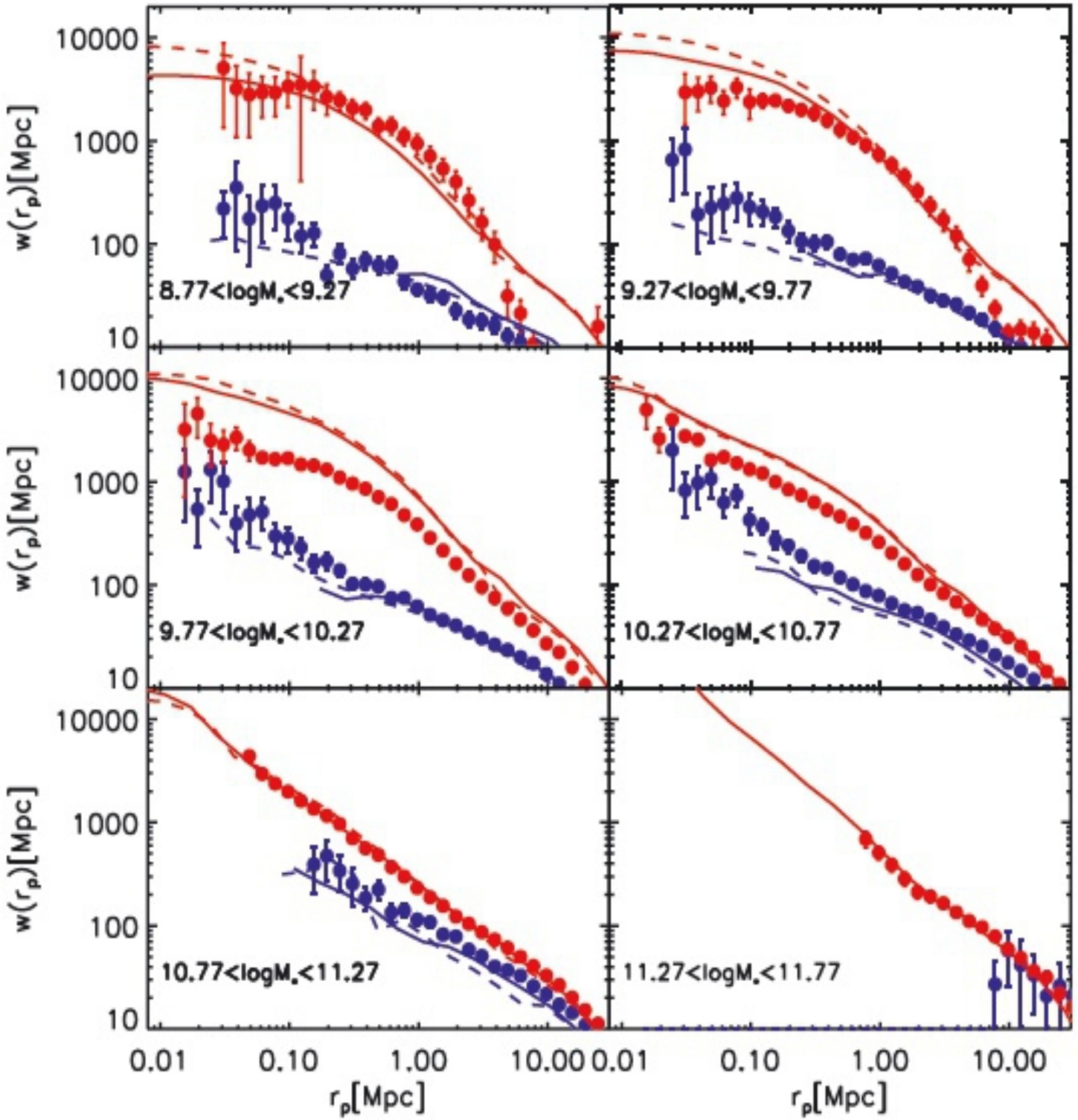
10000
1000
100
10
w(r_p)[Mpc]
8.77<logM*<9.27
9.27<logM*<9.77
9.77<logM*<10.27
10.27<logM*<10.77
10.77<logM*<11.27
11.27<logM*<11.77
0.01
0.10
1.00
10.00
r_p[Mpc]

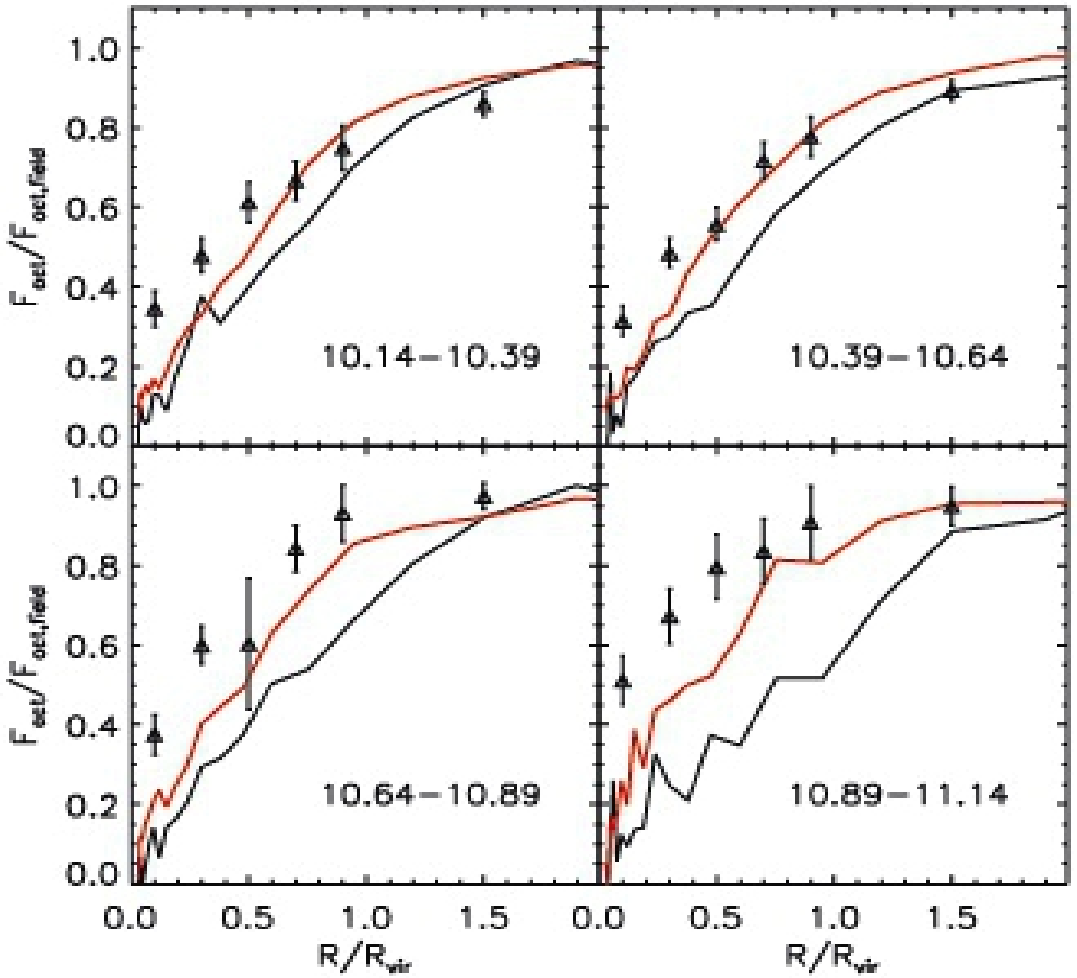

Figure 3. The reduction in the fraction of actively star-forming galaxies ($\dot{M}_*/M_* > 10^{-11}$ yr^{-1}) as a function of the projected distance from the cluster centre in units of $R_{\rm vir}$. The four panels refer to different ranges of $\log M_*/M_\odot$ as indicated by the labels. Predictions from the preferred model of this paper applied to the MS are shown in red and those from the model of DLB07 are shown in black. Symbols with error bars are SDSS data for a large sample of nearby clusters taken from Weinmann et al. (2010). For each curve, the fraction of actively star-forming galaxies is normalized by its 'field' value, taken to be the value at $2R_{\rm vir}$. This emphasizes the effect of cluster environment on star formation activity.